AD-A182 320 SUBMERGED STRUCTURAL RESPONSE TO WEAK SHOCK BY COUPLED THREE-DIMENSIONAL.. (U) NAVAL RESEARCH LAB WASHINGTON DC M A TAMM ET AL. 21 MAY 87 NRL-MR-5903 1/1

UNCLASSIFIED F/G 13/13 NL

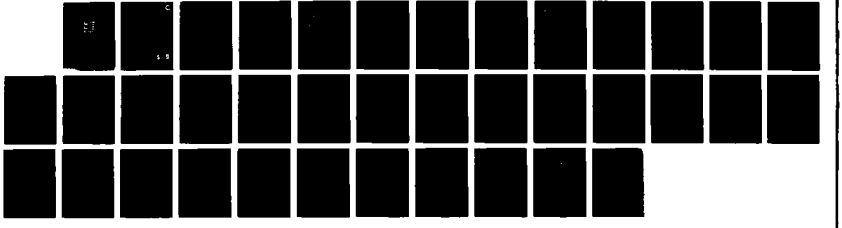

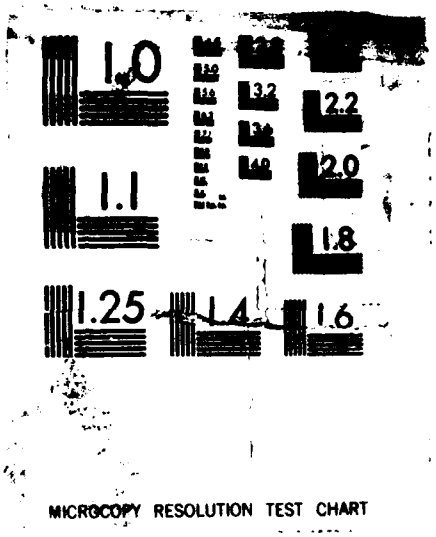

MICROCOPY RESOLUTION TEST CHART

Naval Research Laboratory
Washington, DC 20375-5000

NRL Memorandum Report 5903

Submerged Structural Response to Weak Shock by Coupled Three-Dimensional Retarded Potential Fluid Analysis—Finite Element Structural Analysis

MARTIN A. TAMM AND WAYLON W. WEBBON*

Structural Integrity Branch
Material Science and Technology Division

**Martin Marietta Baltimore Aerospace*
Baltimore, MD

May 21, 1987

AD-A182320

SECURITY CLASSIFICATION OF THIS PAGE

REPORT DOCUMENTATION PAGE

1a. REPORT SECURITY CLASSIFICATION UNCLASSIFIED	1b. RESTRICTIVE MARKINGS
2a. SECURITY CLASSIFICATION AUTHORITY	3. DISTRIBUTION / AVAILABILITY OF REPORT Approved for public release; distribution unlimited.
2b. DECLASSIFICATION / DOWNGRADING SCHEDULE	
4. PERFORMING ORGANIZATION REPORT NUMBER(S) NRL Memorandum Report 5903	5. MONITORING ORGANIZATION REPORT NUMBER(S)
6a. NAME OF PERFORMING ORGANIZATION Naval Research Laboratory 6b. OFFICE SYMBOL (If applicable) Code 6330	7a. NAME OF MONITORING ORGANIZATION
6c. ADDRESS (City, State, and ZIP Code) Washington, DC 20375-5000	7b. ADDRESS (City, State, and ZIP Code)
8a. NAME OF FUNDING / SPONSORING ORGANIZATION 8b. OFFICE SYMBOL (If applicable)	9. PROCUREMENT INSTRUMENT IDENTIFICATION NUMBER
8c. ADDRESS (City, State, and ZIP Code)	10. SOURCE OF FUNDING NUMBERS PROGRAM ELEMENT NO. 61153N; PROJECT NO RR023-45; TASK NO; WORK UNIT ACCESSION NO DN080-050

11. TITLE (Include Security Classification)
Submerged Structural Response to Weak Shock by Coupled Three-Dimensional Retarded Potential Fluid Analysis--Finite-Element Structural Analysis

12. PERSONAL AUTHOR(S) Tamm, Martin A. and Webbon, Waylon W.*

13a. TYPE OF REPORT	13b. TIME COVERED	14. DATE OF REPORT (Year, Month, Day)	15. PAGE COUNT
Final	FROM 10/83 TO 9/84	1987 May 21	37

16. SUPPLEMENTARY NOTATION
*Martin Marietta Baltimore Aerospace, Baltimore, MD

17 COSATI CODES			18. SUBJECT TERMS (Continue on reverse if necessary and identify by block number)
FIELD	GROUP	SUB-GROUP	Retarded potential integral, Fluid structure interaction, Coupled field analysis, Submerged structural response

19. ABSTRACT (Continue on reverse if necessary and identify by block number)

The discretized Kirchhoff retarded potential integral equation for solving the linear acoustic wave equation is coupled to a general finite element structural analysis code to model underwater vibrations. Arbitrary three dimensional problems can be handled, with a present restriction on the allowed orientation of the finite element grid lines and the requirement of a plane wave form. Ramp and Fourier series approximations to a step wave are applied to rigid and elastic spheres to test the numerical formulation, and to test the validity of using a continuous approximation to a discontinuous loading.

Keywords:

20. DISTRIBUTION / AVAILABILITY OF ABSTRACT	21. ABSTRACT SECURITY CLASSIFICATION
☒ UNCLASSIFIED/UNLIMITED ☐ SAME AS RPT ☐ DTIC USERS	UNCLASSIFIED
22a. NAME OF RESPONSIBLE INDIVIDUAL Martin A. Tamm	22b. TELEPHONE (Include Area Code) (202) 767-3505 22c. OFFICE SYMBOL Code 6330

DD FORM 1473, 84 MAR 83 APR edition may be used until exhausted
All other editions are obsolete

SECURITY CLASSIFICATION OF THIS PAGE

GU.S. Government Printing Office 1985-607-047

CONTENTS

SUBMERGED STRUCTURAL RESPONSE TO WEAK SHOCK BY COUPLED THREE-DIMENSIONAL RETARTED POTENTIAL FLUID ANALYSIS—FINITE ELEMENT STRUCTURAL ANALYSIS

INTRODUCTION

This study is a continuation of the effort to apply the retarded potential integral to increasingly general classes of problems in fluid-structure interaction. Mitzner [1,2] developed a method for discretizing the integral spatially and temporally, and applied the technique to the problem of a spherical rigid, immovable body impinged by a plane pressure wave with a smooth waveform. Huang, Everstine, and Wang [3] extended the method to handle a non-rigid boundary condition, and tested the case of a spherical elastic shell, modeled with axisymmetric shell elements, impinged by a plane step wave. However, the special problem posed for the integral formulation by a pressure discontinuity was handled by solving the rigid scattering portion of the problem closed-form using separation of variables. Neilson, Lu, and Wang [7] directly tackled the problem of the discontinuous shock wave front for rigid body problems and axisymmetric surfaces using the wavefront line integral term.

This work builds upon the computer program developed by Mitzner and extended to non-rigid boundaries by Huang, Everstine, and Wang. A fully three-dimensional boundary element formulation for arbitrary shaped surfaces has been implemented. The entire method is designed to be compatible with finite element methods and has been linked to the ADINA finite element program. Continuous pressure loadings can be successfully used to approximate loading discontinuities, avoiding the difficulties inherent in the wavefront line integral approach.

A concurrent effort in the creation of a general three-dimensional analysis capability is the development of a parametric patch surface geometry definition for the retarded potential integral. This allows arbitrarily shaped surfaces to be specified by the coordinates of a finite number of points, as is done with finite elements. This development is described in a related report [10], and is used in the computations described in this report.

RETARDED POTENTIAL FORMULATION

The retarded potential integral is the solution of the linear wave equation,

$$\nabla^2 p = \frac{1}{c^2} \frac{\partial^2 p}{\partial t^2}$$

subject to the boundary condition, $\partial p / \partial n = -\rho \ddot{w}$. This is the governing differential equation for a linearly compressible, inviscid fluid with negligible changes in density. The assumption of linear fluid behavior is said to be accurate for pressures up to 30,000 psi [9].

A discussion of the retarded potential equation and its discretized approximation as applied to the submerged structural problem may be found in Refs. [1,2,3]. A good derivation is found in Ref. [4]. The form of the equation for calculation of total pressures, p, on a bounding surface in an infinite fluid subject to a continuous incident pressure field loading, p^{inc}, is as follows:

Manuscript approved December 17, 1986.

$$p(\bar{x},t) = 2p^{inc}(\bar{x},t) - \rho/2\pi \int_S \frac{\ddot{w}(\bar{x}',t')}{R}\, dS'$$

$$+1/2\pi \int_S \left\{ p(\bar{x}',t') + \frac{R}{c}\frac{\partial p}{\partial t'}(\bar{x}',t') \right\} \frac{1}{R^2}\,\frac{\partial R}{\partial n'}\, dS'$$

$$\text{where} \quad t' = t - \frac{R}{c}$$

$$\text{and} \quad R = |\bar{x} - \bar{x}'|$$

and where

$\bar{x}$ is the position of a field point on the surface,

$\bar{x}'$ is the location of an integration point on the surface,

t' is the retarded time of the influence of field quantities and the integration point,

ρ is the fluid density,

c is the sonic velocity in the fluid,

n' represents the surface normal direction at an integration point oriented out of the fluid,

$\ddot{w}'$ is the normal direction acceleration of the surface oriented out of the fluid.

IMPLEMENTATION

For computation, the retarded potential integral must be discretized and, for a non-rigid bounding structure, linked to a structural analysis code. The surface pressure field is approximated by subdividing the surface into zones of constant pressure coinciding with individual finite element surfaces, and with the surface normal acceleration field also approximated as constant on the same zonal surface. This normal acceleration is obtained from the finite element computation by averaging the acceleration vectors from the corner nodes of each finite element and using the component normal to the center of the zone. Pressures are discretized in time to coincide with the time steps of the finite element program. Prior to conducting the time history computation of pressures and structural vibrations, a matrix of influence coefficients must be calculated that expresses the dependence relations of current pressures on past pressures and past and present accelerations.

First, the time derivative of pressure must be formulated in terms of pressures. A three-point backward difference formula is used in this implementation. Then, for each zone, pressure and acceleration can be factored out of the integral expressions. There is a need, however, to subdivide the zones into a mesh of subzone elements in order to accurately numerically integrate the geometric influence factors, as well as to accurately obtain the time-delay of pressure influences from all parts of the structure. For the purpose of measuring the distance between integration and field points and thereby the time-retardation, the field point is located at the center of the field zone and the integration point is located at the center of the subzone integration element. The exception to this rule is that the influence of the singular integration element, which surrounds the field point, is lumped at a distance from the field point of one-fourth the diagonal dimension of the singular element. The integration points will not fall at a whole number of time intervals from the field point, so an interpolation from adjacent whole time intervals is needed to determine the pressure at the integration point.

Fundamental Relationships in the Discretization

Definitions:

$\bar{x}$ - position vector

R - distance between integration and field points

j - field point (and zone) index

k - integration zone index

l - subzone element index

(k,l) - integration point indices

c - wave velocity

t - current time

t' - retarded time

τ - time step size

m - time step index

m' - time step index of retarded time (not a whole number)

i - generic index of time retardation or delay

i'_{jkl} - number of time steps of delay in the influence of integration point (k,l) on field point j (not a whole number)

Pressure:

$$p_{jm} = p(\bar{x}_j, m\tau)$$

$$p_{klm'} = p(\bar{x}_{kl}, m'\tau)$$

Acceleration:

$$\ddot{w}_{jm} = \ddot{w}(\bar{x}_j, m\tau)$$

$$\ddot{w}_{klm'} = \ddot{w}(\bar{x}_{kl}, m'\tau)$$

Distance:

$$R_{jkl} = |\bar{x}_j - \bar{x}_{kl}|$$

Retarded Time:

$$t' = t - R/c$$

$$m'\tau = m\tau - R_{jkl}/c = m\tau - i'_{jkl}\tau$$

Time Retarded Pressure, Acceleration, and Pressure Derivative in terms of pressures and acceleration at whole time steps:

$$p_{k,m-i'_{jkl}} = \sum_i f_{jkli}\, p_{k,m-i}$$

$$\ddot{w}_{k,m-i'_{jkl}} = \sum_i f_{jkli}\, \ddot{w}_{k,m-i}$$

$$\tau \left(\frac{\partial p}{\partial t'} \right)_{k,m-i'_{jkl}} = \sum_i f^{\bullet}_{jkli}\, p_{k,m-i}$$

where, for linear interpolation of field quantities between whole time steps,

$$f_{jkl} = 1 - |i - i'_{jkl}|, \text{ when } 1 > i - i'_{jkl} > -1$$

$$f_{jkl} = 0, \text{ otherwise}$$

and, for the 3-point backward difference discretization of the pressure derivative,

$$f^{\bullet}_{jkl} = \frac{3}{2} f_{jkl} - 2 f_{jkl,i-1} + \frac{1}{2} f_{jkl,i-2}$$

Retarded Potential Integral:

$$p_{jm} = 2p^{inc}_{jm} - \frac{\rho}{2\pi} \sum_{k,l} \ddot{w}_{k,m-i'_{kl}} \left(\int_{S_{kl}} \frac{dS'}{R} \right)_{jkl}$$

$$+ \frac{1}{2\pi} \left\{ \sum_{k,l} p_{k,m-i'_{kl}} + i'_{jkl} \tau \left(\frac{\partial p}{\partial t'} \right)_{k,m-i'_{kl}} \right\} \left(\int_{S_{kl}} \frac{1}{R^2} \frac{\partial R}{\partial n'} dS' \right)_{jkl}$$

Inserting the above expressions for time retarded pressures, accelerations, and pressure derivatives into the discrete Retarded Potential Integral, summing over the l index, and consolidating the time-independent factors into matrices called A and B, results in an expression of the form,

$$(1 - B_{jj0})\, p_{jm} = 2p^{inc}_{jm} + \sum_{k,l} A_{jkl}\, \ddot{w}_{k,m-i} + \sum_{k,l} B_{jkl}\, p_{k,m-i}$$

which allows the current pressures p_{jm} to be computed from past pressures and current and past accelerations.

The particular approximations used for the geometric influence factors, $\left(\int_{S_{kl}} \frac{dS'}{R} \right)_{jkl}$ and $\left(\int_{S_{kl}} \frac{1}{R^2} \frac{\partial R}{\partial n'} dS' \right)_{jkl}$, depend on whether or not the integration element, (k,l), is singular with respect to field point, j. This is discussed further in Ref. 10.

The numerical integration over the subzone elements is a subject left to the related paper concerning a parametric surface patch basis for the geometric calculations of the method [10]. The original formulation of the numerical integration is presented in [1,2].

A staggered solution technique is used in the analysis so that for each time step the structural and fluid dynamic problems can be solved alternately rather than concurrently, greatly simplifying computation, yet nearly preserving the simultaneity of the two problem solutions. For the step by step solution of the fluid-structure interaction problem, the cycle of computation is as follows:

0. At time step 0, initialize $p_{j0} = 0$

1. At time step m, $t_m = m\tau$. Apply pressures, p_{jm} to structural model.

2. Calculate accelerations, $\ddot{w}_{j,m+1}$, at time t_{m+1}, from structural model.

3. Calculate pressures, $p_{j,m+1}$, at time, t_{m+1}, with integral equation, due to $p^{inc}_{j,m+1}$; $\ddot{w}_{j,m+1}$; $\ddot{w}_{m+1-i}$; (the time retarded surface accelerations; and p_{m+1-i} (the time retarded surface pressures).

4. If $m+1$ is the last desired time step, stop the solution.

5. Increment m. Go to computational step 1.

The computational cycle is depicted in Fig. 1, showing the relationships among the processes and the data input and generated. From the point of view of the retarded potential calculations there are two independent inputs: the incident wave loading and the surface accelerations. It is sometimes convenient to think separately of the pressure field contributions of these inputs. For this purpose, the reflection of the incident wave off a rigid, immovable body is referred to as the scattered field, and the incremental pressure field produced by motion of the surface alone is called the radiated field. The incident wave field and scattered field together are known as the rigid body pressure field.

The subzone division used in calculating the time-delayed influences of surface pressures on each other varies with the distance between pressure zones. In the current implementation the refinements of subzone meshes are: 1. Coarse, 2. Fine, and 3. Singular zone meshing. The coarse meshing is used for two zones that are remote from each other; the fine mesh for two zones near each other; and the singular zone mesh for calculating the influence of a pressure zone on itself.

INCIDENT WAVE

Simple incident wave definitions can be given for plane and spherical waves. The incident field for a plane wave is defined by specifying a time history of the incident pressure on one plane in space, the coordinates of one point on the plane, and the direction of wave travel normal to the plane. Then the pressure history at any other point is time-delayed by the travel time to the point from the defining plane. This relationship is expressed as

$$p(\bar{x},t) = p_o(t - (\bar{x}-\bar{x}_o)\cdot\bar{i}/c)$$

where $p(\bar{x},t)$ is pressure at point $\bar{x}$ at time

p_o is the pressure history at $\bar{x}_o$,

$\bar{i}$ is the incident wave direction,

c is the wave velocity.

For a spherical wave, the pressure history is given for one spherical mathematical surface surrounding the source of the wave, and the coordinates of the source and the radius to the defining surface. Because spherical waves, as they spread, attenuate in proportion to the inverse radius, this factor must be included in the incident pressure calculations. The pressure expression is as follows:

$$p(\bar{x},t) = (R/r)\, p_R(t - (r-R)/c)$$

where $r = |\bar{x}-\bar{x}_o|$, the distance from the pressure source,
and p_R is the pressure history at radius R from the wave source.

All pressures prior to the arrival of the incident wave are set to zero.

At present only the plane wave option is installed in the program, but the spherical wave option is easily added.

NUMERICAL RESULTS

The two basic problems investigated for the three-dimensional technique are a submerged rigid immovable sphere in an infinite fluid field, and an elastic spherical shell in the same environment. Each is subject to the same planar step wave. No gravity is included in the models. Comparisons are made of different approximations of a step wave. The problem dimensions and properties are as follows:

shell radius-to-thickness ratio $a/h = 50$,

shell-to-fluid density ratio $\rho_s/\rho_w = 7.80$,

modulus ratio $E/\rho_w c^2 = 97$,

Poisson's ratio $\nu = 0.3$.

The structural model for both problems is shown in Fig. 2. This is a quarter section of a sphere used to model an entire spherical shell with symmetry conditions imposed on the two cutting planes. Both the retarded potential program and the ADINA finite element program allow for such symmetry conditions. The symmetries were imposed to save computation cost and can be allowed because both the test structure and the test loadings are axisymmetric with respect to the loading direction. The subdivision into pressure zones and finite elements is more refined in the direction of wave travel in order to capture the more detailed behavior variations expected in that direction. The particular zone subdivisions used in this study are shown in Fig. 3. A fine mesh is used throughout the interzone influence calculations.

The Rigid Scattering Problem

The retarded potential technique was first studied for the rigid scattering problem, independent of the structural analysis code, to verify the 3-dimensional integration method under shock loading. Pictorially, this is equivalent to removing the left side of the problem illustrated in Fig. 1 and setting the accelerations identically to zero.

In choosing continuous approximations to a discontinuous step wave loading, three considerations are: 1. the approximation should accurately capture the shape and peak values of the surface pressures and structural response; 2. the loading should induce a minimal amount of numerical instability in the computation; and 3. the loading data should be easy to generate. The three loading approximations tested in this study are a linear ramp, one half of a sine squared waveform, and a Fourier series. Because the sine squared approximation was found to yield the same solution behavior characteristics as the ramp function, the following discussion will be limited to the ramp and Fourier series. The motivation for trying the Fourier series approximation is to eliminate higher frequency components in the loading that might initiate or aggravate numerical instabilities.

For each loading type, variation can be made in the steepness of the approximation to an absolute step. For the ramp loading, this is a variation in the number of time steps to reach peak load, and for the Fourier series, a variation in the highest frequency present. There is a tradeoff between solution accuracy and solution stability; the steeper loadings give more accurate but less stable responses. A variety of loading steepnesses were tried, and the ones found to give the best compromise between accuracy and stability are: a ramp loading allowed to rise to maximum pressure in 5 time steps, and a Fourier series approximation including frequencies up to 600 Hz in 1 Hz intervals. The loadings are plotted in Fig. 4. Computations were carried out to 20 non-dimensional times ($T = c\tau / a$) to fully test the stability of the responses. Because the response in all cases reaches a steady state by five non-dimensional times, the results of the rigid body study are plotted for this length of time in Figs. 6 with the location of the plotted points shown in Fig. 5. At one location the response is plotted out to a full 20 non-dimensional times to show the later stability behavior of the computation, typical of all locations.

The standard of comparison used in the rigid body study is the eight-term Legendre series solution from Huang [11]. As can be seen, both loadings give accurate pressure histories on the surface at all points. The ramp loading characteristically gives sharper pressure peaks than the Fourier series loading and higher maximums. Theoretically, the illuminated half of the sphere should experience a peak of twice the unit step pulse. The approximate loadings do not achieve this maximum because the peak loading pressure is reached over a period of time rather than instantaneously, allowing the scattered wave time to dissipate. The ramp loading characteristically has a high frequency, low amplitude oscillation superimposed on the solution. This does not, however, lead to divergence. The computations for neither case diverge over the 20 non-dimensional times for which the test was run. The undulating approximations to zero pressure that the Legendre series solution and the Fourier loading response exhibit prior to the actual arrival of the wave at a given surface point, are artifacts of the series approximations. This is particularly evident in the higher θ angles (Figs. 6).

A new stability consideration was discovered for the computations. It was observed that the time step size and the subzone mesh size should be appropriately matched to obtain stable solutions. The stability requirement was established in previous studies that the distance from an integration point in one pressure zone to the field point in another zone should be at least a full time step to prevent an instantaneous pressure influence from one zone to the next. However, it is now also

apparent that the time step should not be small relative to the subzone integration elements. This is to prevent lumping of integration element influences at widely separated time steps, leaving intermediate time steps with no apparent influence. This possibility can arise because the subzone element influence is lumped at the center of the element prior to lumping the influences at the discretized retarded times. The preferred relationship is to have a time step transit distance somewhat smaller than the closest distance between any pair of integration and field points which are in different zones, but stability problems occur only with gross disparity in sizes. This area warrants further study.

Submerged Elastic Structural Response

For the combined problem of fluid and elastic structural dynamics, the same spherical geometry and plane step pressure loading is used as for the rigid body problem. A thin elastic shell of diameter-to-thickness ratio, 100, is modeled with 9-noded quadrilateral shell finite elements. The identical mesh is used for the finite element modeling of the structure as for the discretization into constant pressure zones, in accordance with the implementation. The simulation of structural response to the plane step wave is carried out for a period of 20 non-dimensional times beyond the incident wave's initial impact with the sphere. The same non-dimensional time step of 0.05 is used as for the rigid body problem. A consistent mass formulation is used in the finite element model and has been found essential to the accuracy of the solution. No internal structural damping is included.

The resulting history of surface displacements and velocities are plotted in Figs. 8 and 9. Figure 7 illustrates the locations and orientations of these plotted values. The angle, θ, of the location varies from zero at the point of of first wave impact to 180 degrees at the point of deepest shadow. All of the surface displacements plotted are the components perpendicular to the direction of the incident wave travel, and all the velocities are the components in the direction of the incident wave. In these figures, the numerical solutions are compared to a closed-form series solution for a step wave on an elastic sphere obtained by separation of variables from Ref. [3,8]. The same two loading cases considered for the rigid body case are compared: a five time step ramp approximation of the step wave, and a Fourier series approximation consisting of the frequencies from 0 to 600 Hz in 1 Hz increments.

The results show some general trends. The results agree very well in the shape of the plotted response curves, and have good agreement in amplitudes at early time. For both loading approximations, the velocities and displacements exhibit an increasing damping of response with time compared to the series solution. The numerical solutions begin to increasingly oscillate, as well. The oscillations are more noticeable in the velocities than the displacements. It is evident that the velocity oscillations are integrated out in the displacements.

A few exceptions to these trends should be mentioned. The $\theta = 0$ velocity of the ramp loading shows an exaggerated oscillation from the beginning, that, in fact, dies down noticeably before building up again at later time. The Fourier loading doesn't induce this, and its response is rather damped compared to the initial spike in the series solution. At both the point of initial impact and in the deep shadow region, the tendency to oscillate is much stronger than elsewhere, which can be attributed to the higher frequency response of the loading-direction velocities at these points. As one gets closer to $\theta = 90°$, these velocities increasingly represent only the overall body translation, whereas at $\theta = 0$ and 180, there is a large component of local deformation included.

In comparing the response of the two approximate loadings, the results generally are the same, with certain exceptions. First, there is the already mentioned greater early-time oscillations of the ramp loading case. Then, there is a difference in the pattern of later-time oscillations. For the ramp case, the oscillations tend to increase steadily, whereas the Fourier series response exhibits a strong pulsation or beat in the amplitudes. This is particularly evident in the velocities at θ equal to 0, 162, and 180. Even at early time, the ramp loading response has a very fine oscillation. While the retarded potential integral solution for the rigid body is stable for the cases studied and the Newmark numerical integration used in the finite element analysis is unconditionally stable for undamped structural vibration, the combined method exhibits divergence, and numerical damping is required to achieve a solution. Numerical damping by choice of Newmark parameters is successful in stabilizing the solution without appreciably harming accuracy at early time. The numerical instability, composed of

much higher frequencies than the significant response, is damped out faster than the latter. This is because, for a given frequency component of the vibration, the damping causes the solution to decay by a fixed fraction per cycle, and the higher frequency contributions to the vibration die out faster than the lower frequency. However, at later times the stabilized solution does show a considerable reduction in amplitude compared to the closed-form solution, likely caused by the numerical damping.

The ramp loading shows a greater tendency than the Fourier series for instability, given the same set of Newmark parameters. This tendency is quite noticeable in the velocities at early time. However, the Fourier series, in some cases, shows greater instability at later times. The relative instabilities may depend on which loading curve is changing more rapidly at a given time. The ramp has two sharp changes in direction initially and then becomes constant, while the Fourier series continues to fluctuate throughout its loading history. By using greater numerical damping for the ramp loading case, early time stability equal to that of the Fourier series can be obtained with only slight reduction in the amplitudes of the response. For the velocity at $\theta = 0$, the Fourier series still gives a better match of the analytical solution than does the ramp, which oscillates noticeably about the closed-form curve. However, the ramp more closely approximates the initial velocity peak. For the plotted data, the Newmark integration parameters used are $\delta = 0.8$ and $\alpha = 0.4225$. There is a need for further study on the effect of mesh refinement and time step size on solution accuracy and stability, as well as why the combined method is unstable at all. A stability analysis is needed for the Newmark integration procedure that includes the presence of radiation damping.

CONCLUSIONS

This study has demonstrated a fully three-dimensional implementation of a fluid-structure interaction analysis procedure based on the retarded potential integral coupled to a shell finite element program. A continuous wave approximation to a discontinuous step wave has been found to be successful in modeling shock response problems. The method uses techniques which may be applied to arbitrary three-dimensional bodies, linear or non-linear, whose fluid-structure interface is a closed, smooth surface.

Although difficulties have been encountered in the tradeoff between overdamping and oscillatory divergence, the method has been demonstrated to be quite effective. The early time predictions for both the rigid and elastic problems are accurate and have the potential for improved accuracy up to the limit of the modeling refinement to predict higher frequency responses. For the geometry and loading tested, the rigid body problem has proven to be persistently stable, but for the elastic problem there is a numerical divergence at later time.

Further study in the effects of finite element grid size and configuration and subzone mesh division on problem accuracy and stability is needed. This, as well as an investigation of the coupling of the two computational processes, should improve the performance of the method.

REFERENCES

1. K. M. Mitzner, "Numerical Solution for Transient Scattering from a Hard Surface of Arbitrary Shape—Retarded Potential Technique," Acoustical Society of America, Journal, Vol. 42,1967, pp. 391-397.

2. G. W. Soules and K. M. Mitzner, "Pulses in Linear Acoustics," Northrop Nortronics Report ARD 66-60R, November 1966, ONR Code 468, Nonr 4802 (00), AD 643330.

3. H. Huang, G. C. Everstine, Y. F. Wang, "Retarded Potential Techniques for the Analysis of Submerged Structures Impinged by Weak Shock Waves," Computational Methods for Fluid-Structure Interaction Problems, AMD-Vol.26, ASME, 1977.

4. J. A. Stratton, Electromagnetic Theory, 1941.

5. K.-J. Bathe, Finite Element Procedures in Engineering Analysis, 1982.

6. "A Finite Element Program for Automatic Dynamic Incremental Nonlinear Analysis," Report AE 81-1, ADINA Engineering, Watertown, MA., Sept. 1981.

7. H. C. Neilson, Y. P. Lu, Y. F. Wang, "Transient Scattering by Arbitrary Axisymmetric Surfaces," Acoustical Society of America, Journal, Vol. 63, 1978, pp. 1719-1726.

8. H. Huang, "Transient Interaction of Plane Acoustic Waves with a Spherical Elastic Shell," Acoustical Society of America, Journal, Vol. 45, 1969, pp. 661-670.

9. P. H. Rogers, "Weak-shock Solution for Underwater Explosive Shock Waves," Acoustical Society of America, Journal, Vol. 62, 1977, pp. 1412-1419.

10. M. Tamm, "Parametric Patch Surface Geometry Definition for the Three-Dimensional Retarded Potential Technique," NRL Memorandum Report 5904, 1987.

11. H. Huang, Private Communication.

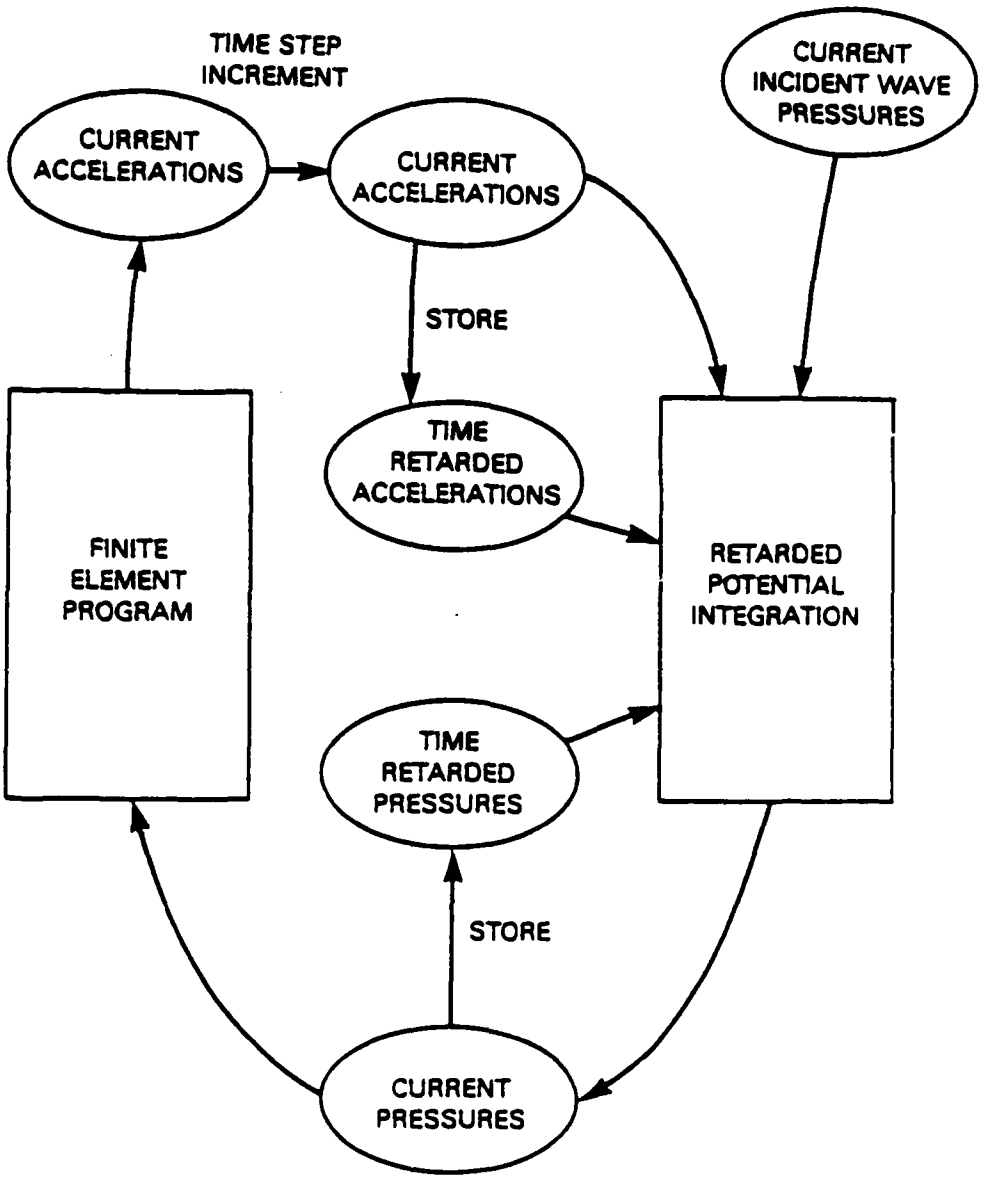

Fig. 1 — Computational Flow

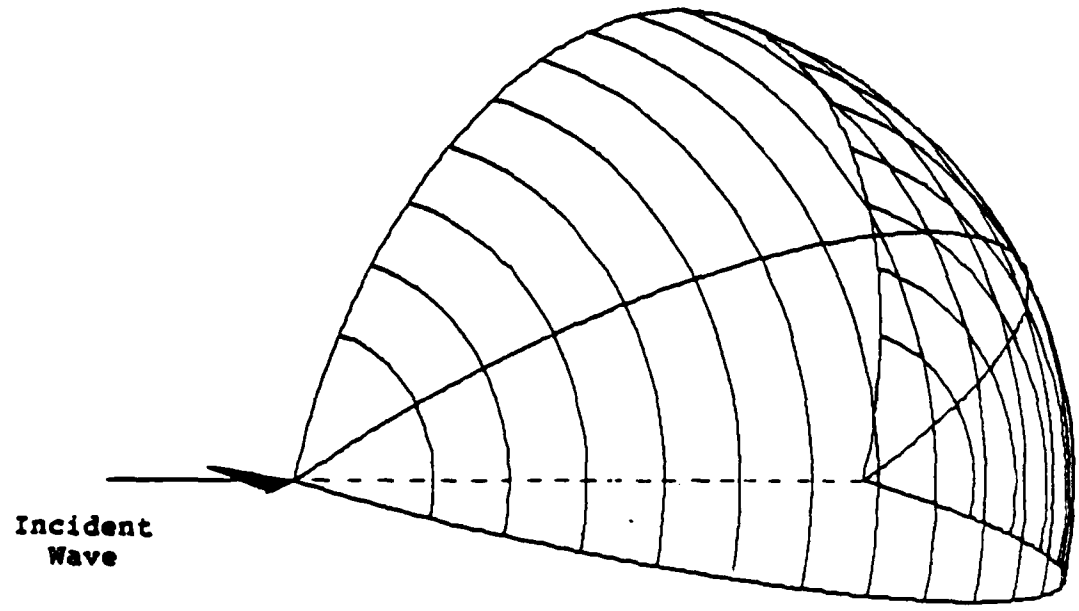

Fig. 2 — Mesh of pressure zones/finite elements

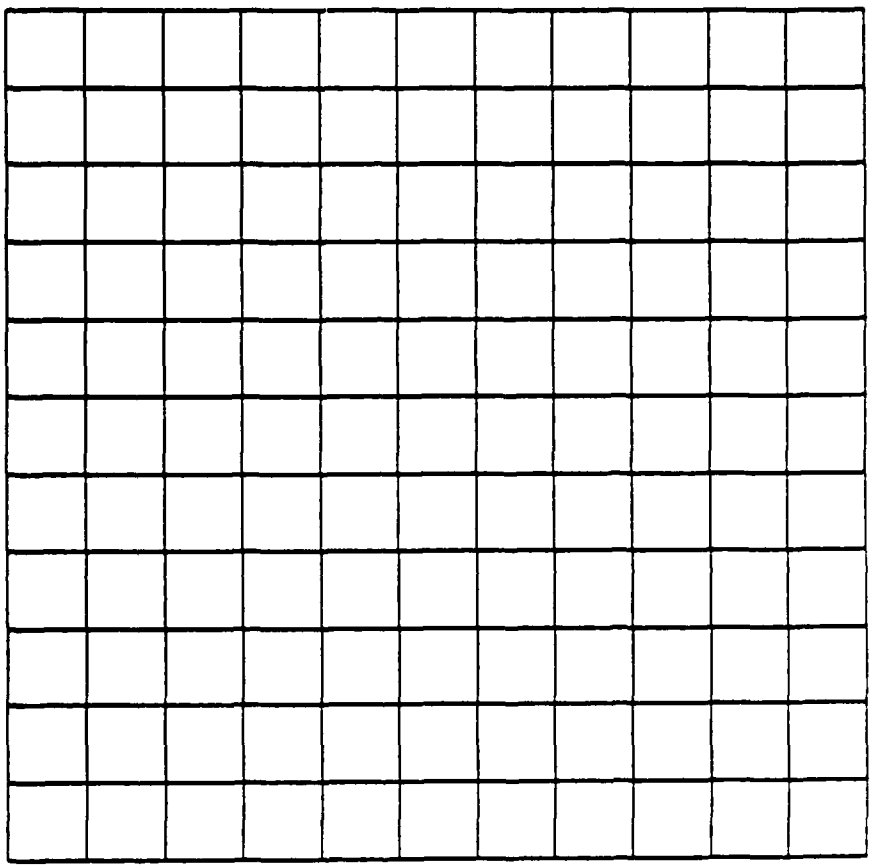

Fig. 3a — Non-singular zone mesh

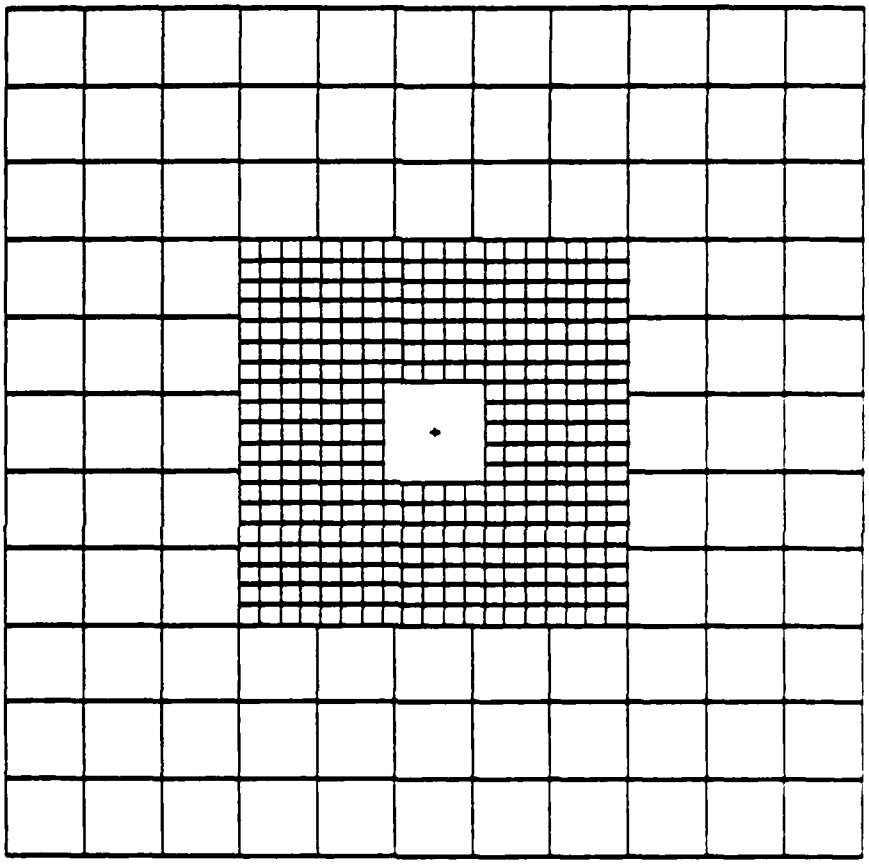

Fig. 3b — Non-singular zone mesh

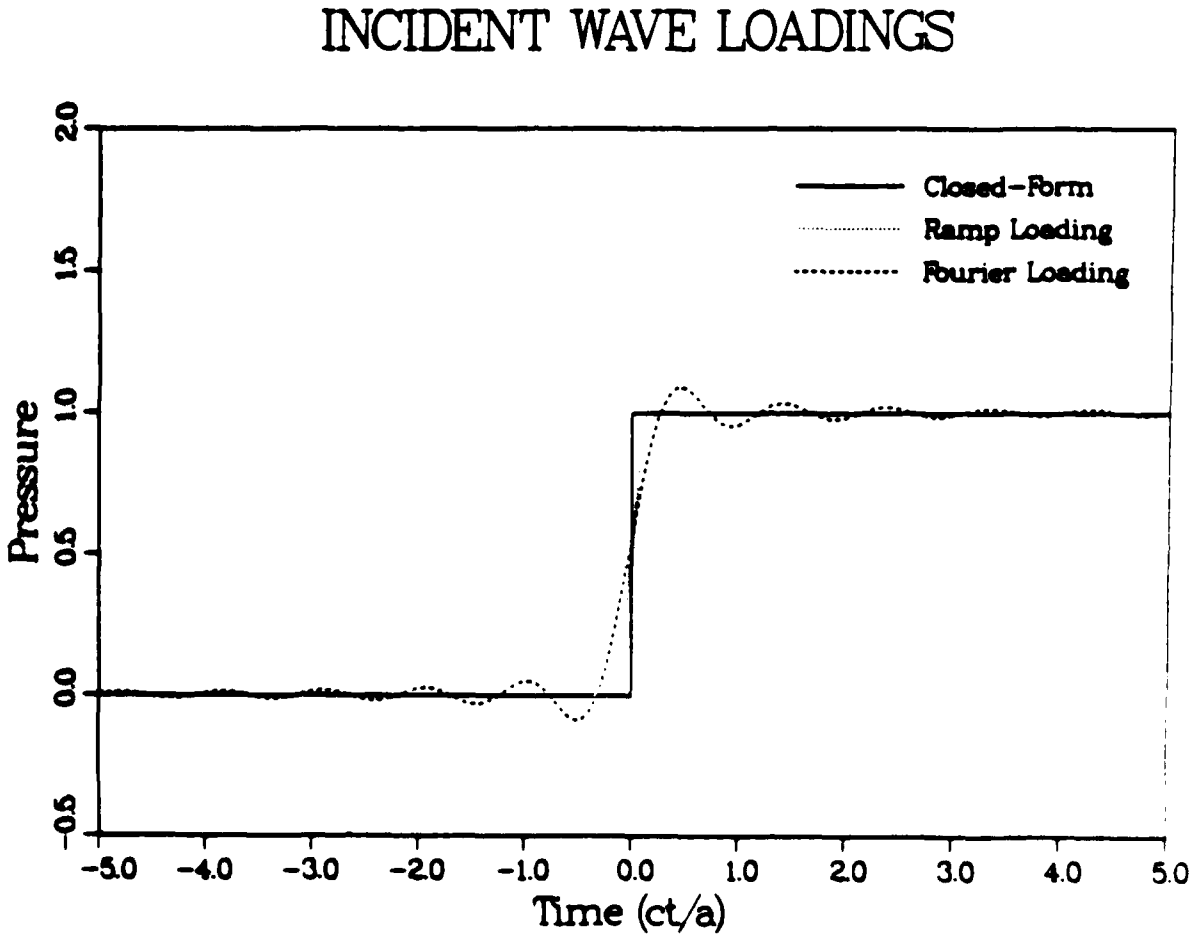

Fig. 4 — Incident wave loadings

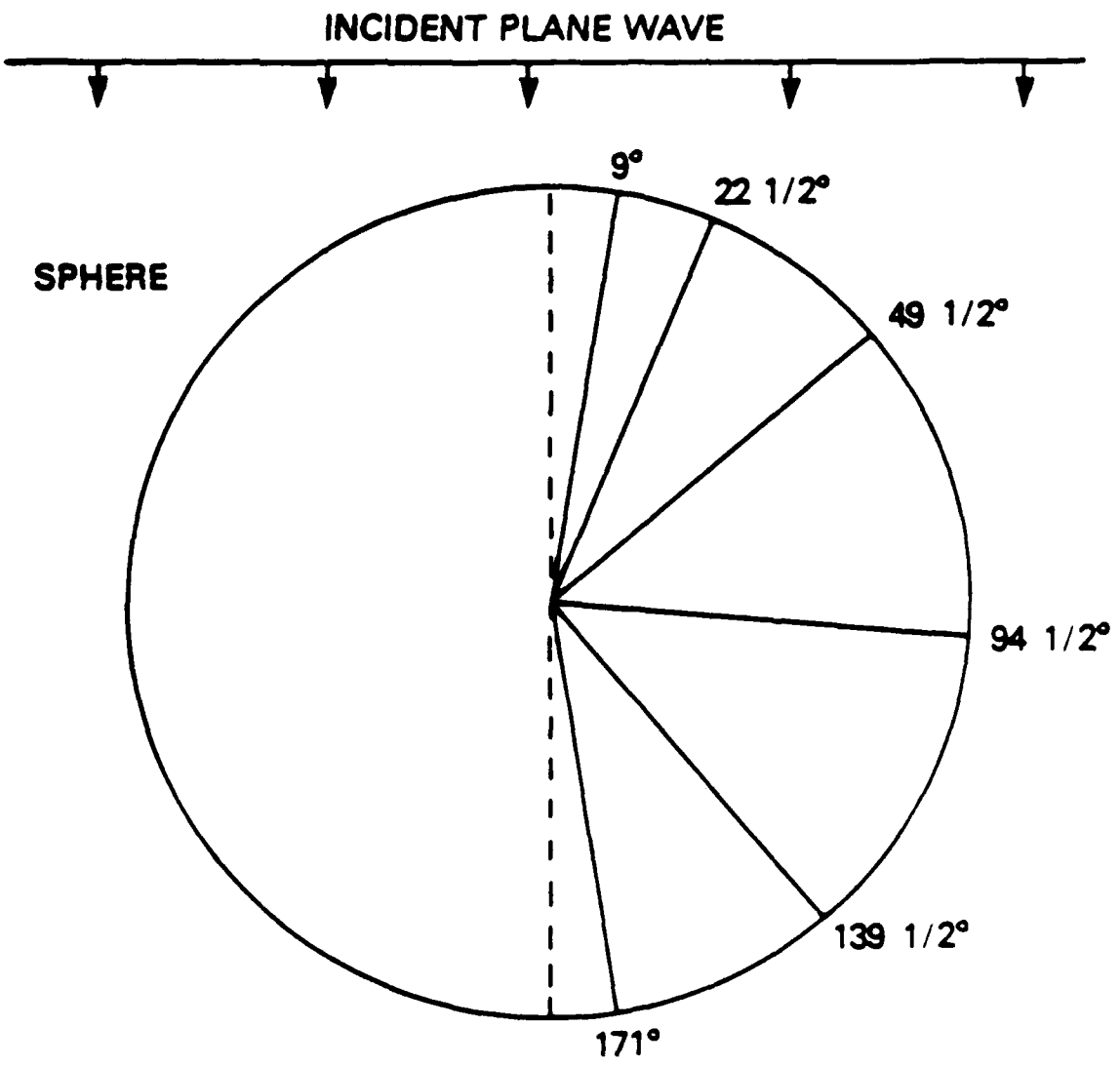

Fig. 5 — Locations of plotted pressures

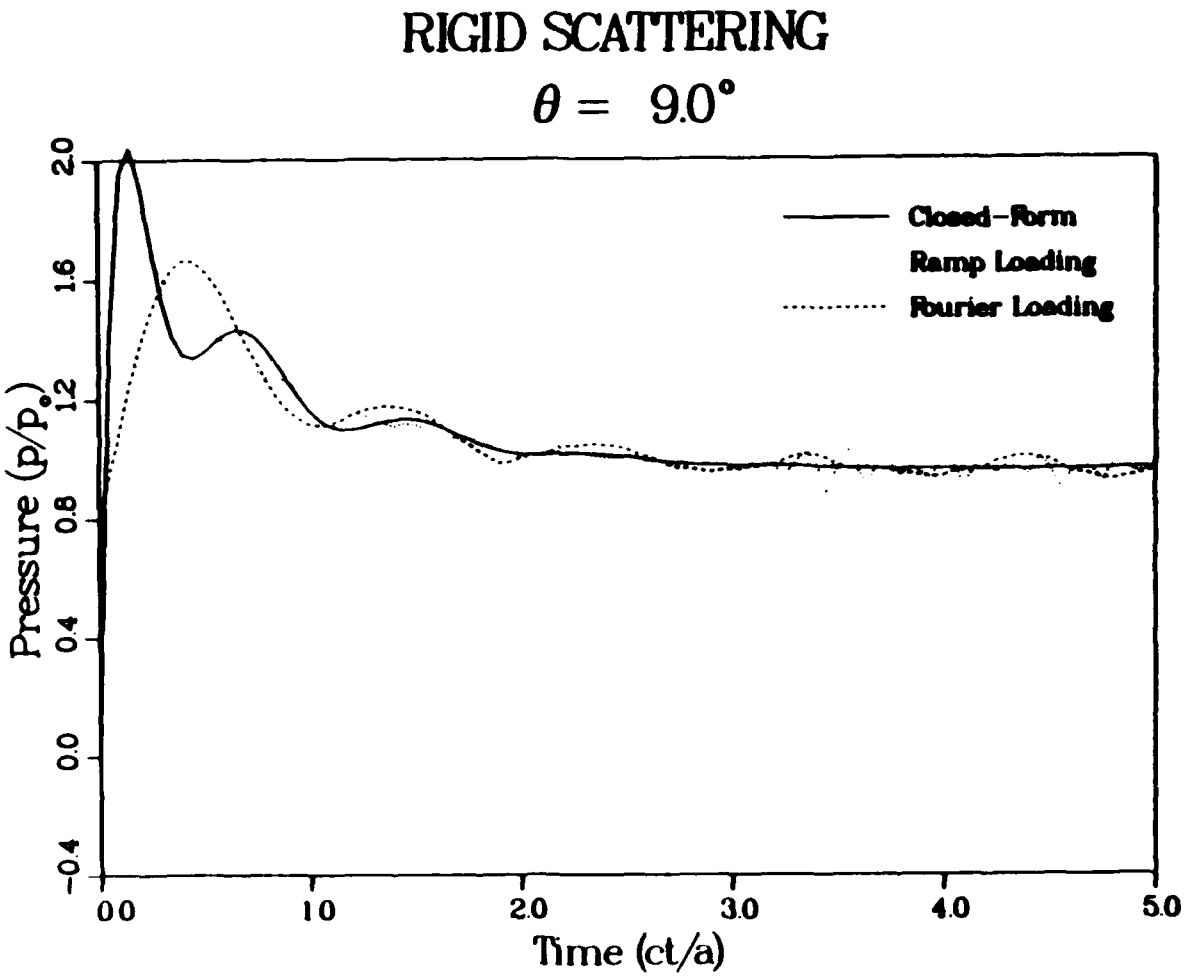
RIGID SCATTERING
θ = 9.0°
Closed-Form
Ramp Loading
Fourier Loading
Pressure (p/p₀)
2.0
1.6
1.2
0.8
0.4
0.0
-0.4
0.0
1.0
2.0
3.0
4.0
5.0
Time (ct/a)

Fig 6a

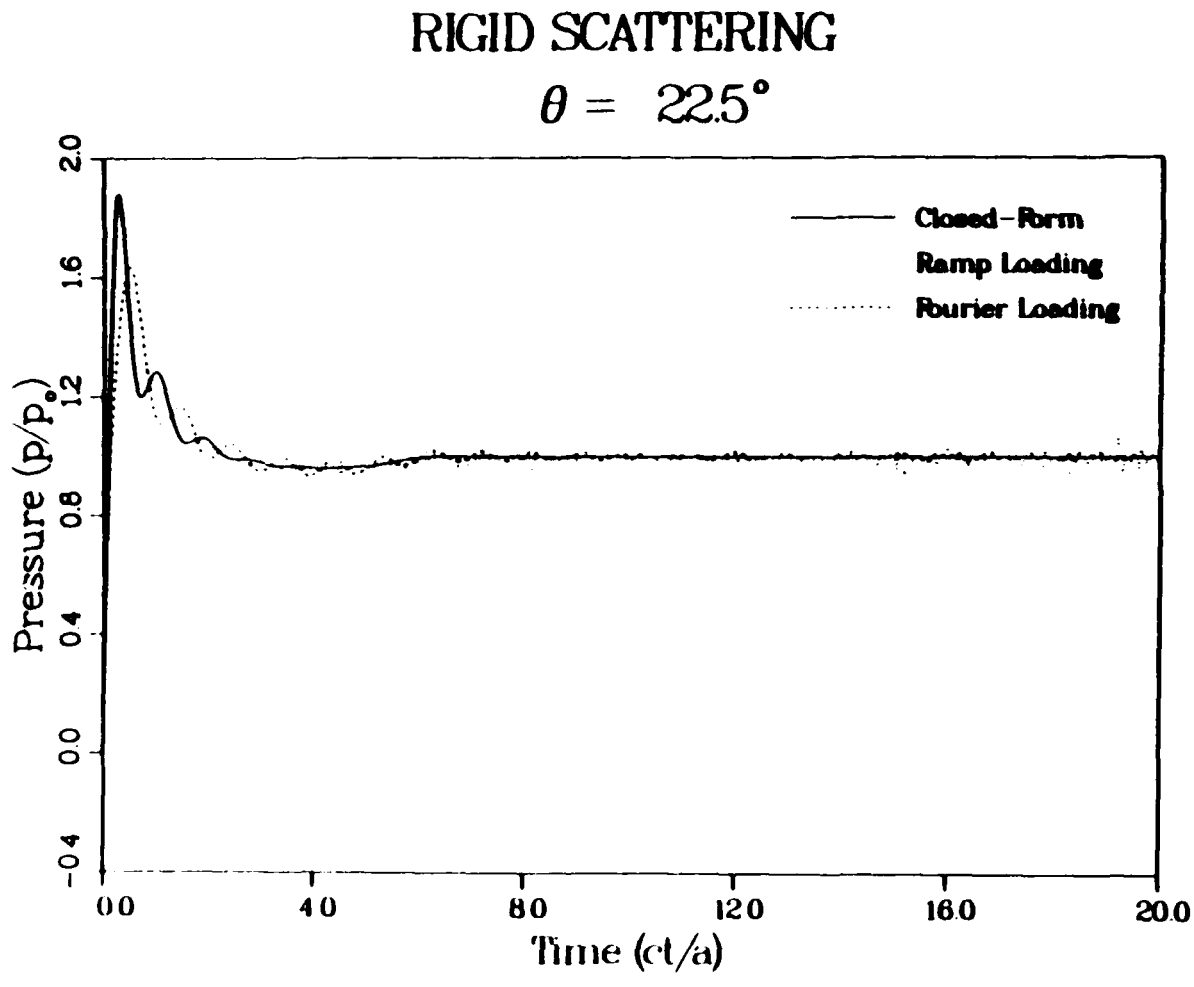
RIGID SCATTERING
θ = 22.5°
Closed-Form
Ramp Loading
Fourier Loading
Pressure (p/p_o)
2.0
1.6
1.2
0.8
0.4
0.0
-0.4
0.0
4.0
8.0
12.0
16.0
20.0
Time (ct/a)

Fig. 6b

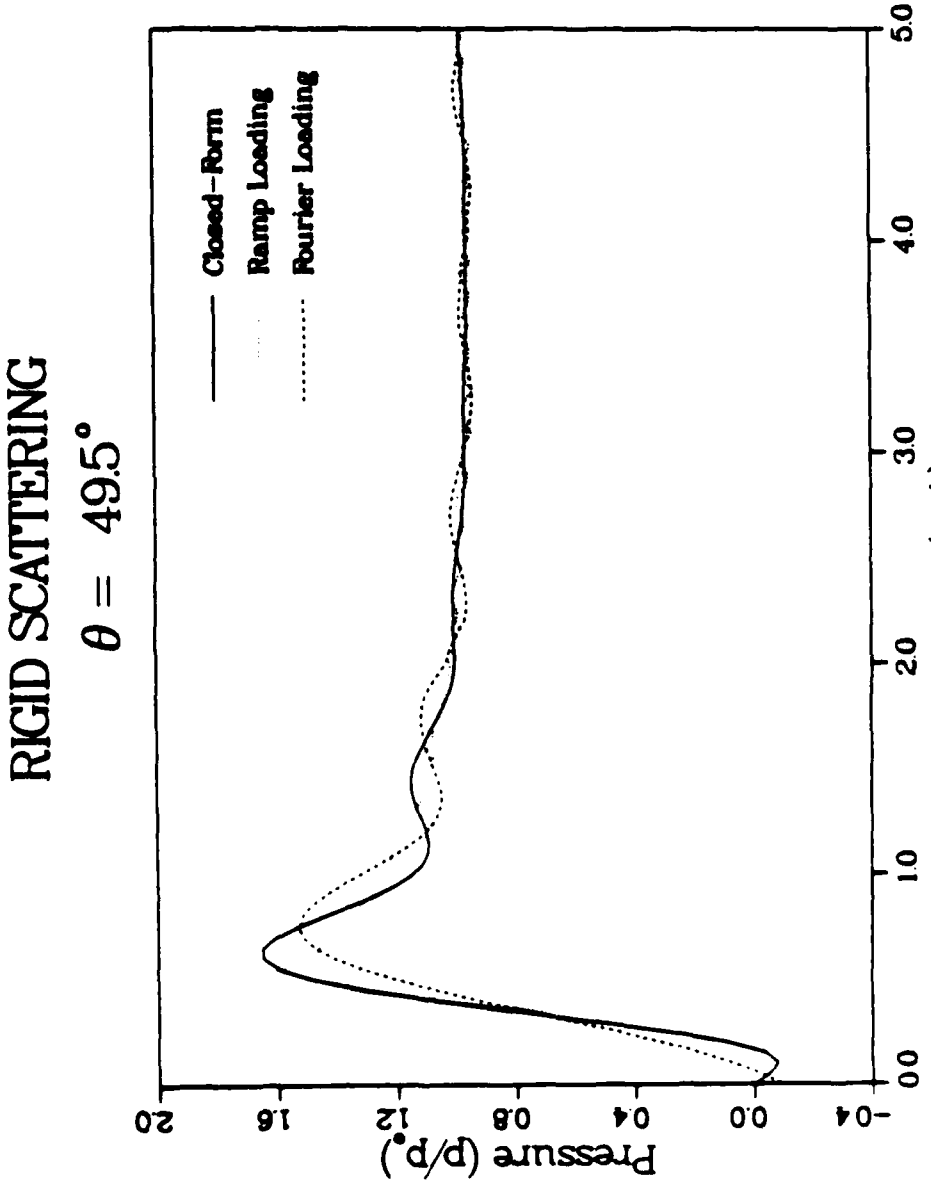
RIGID SCATTERING
$\theta = 49.5°$
Closed-form
Ramp Loading
Fourier Loading
Pressure (p/p_o)
Time (ct/a)
-0.4
0.0
0.4
0.8
1.2
1.6
2.0
0.0
1.0
2.0
3.0
4.0
5.0

Fig. 6c

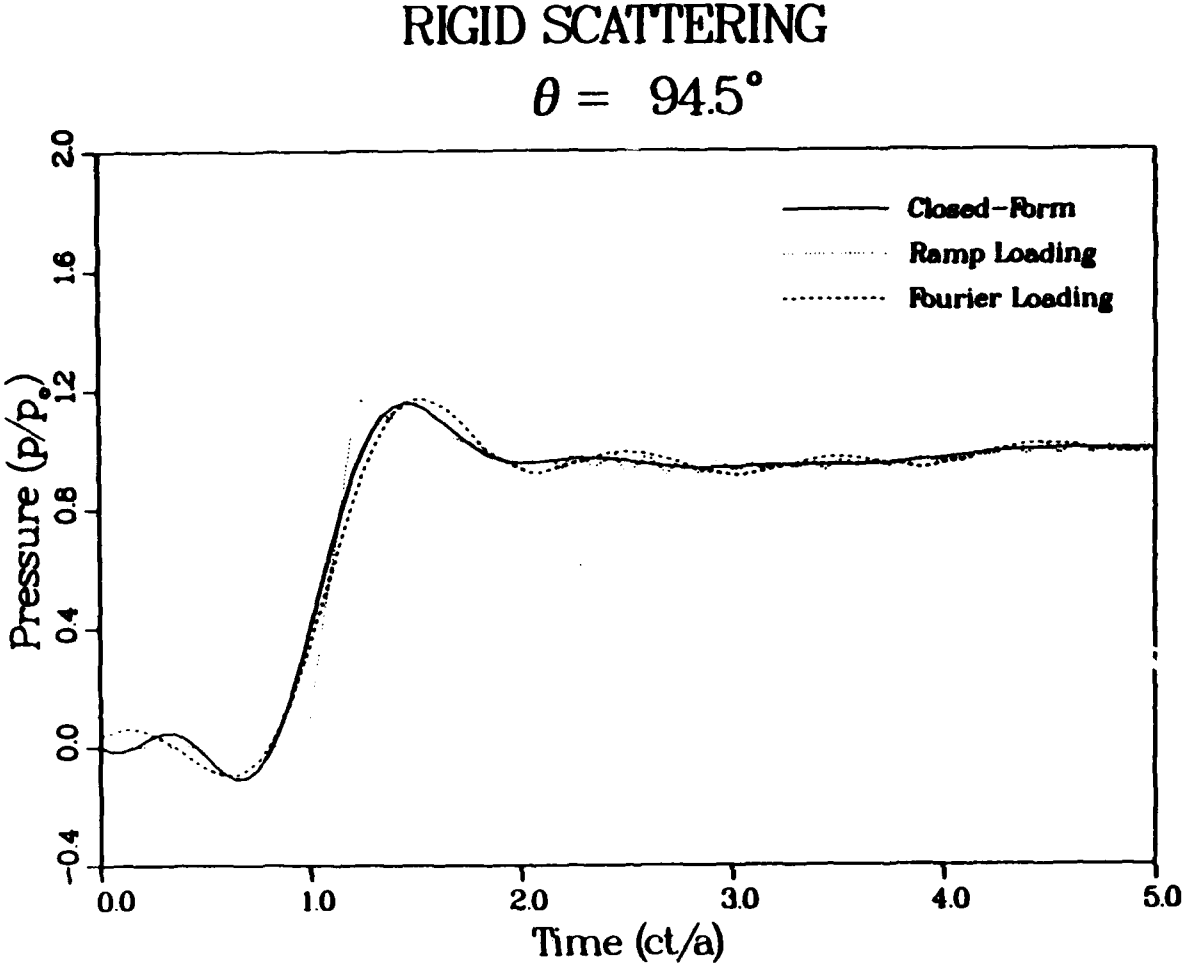
RIGID SCATTERING
θ = 94.5°
Closed-Form
Ramp Loading
Fourier Loading
Pressure (p/p_o)
2.0
1.6
1.2
0.8
0.4
0.0
-0.4
0.0
1.0
2.0
3.0
4.0
5.0
Time (ct/a)

Fig. 6d

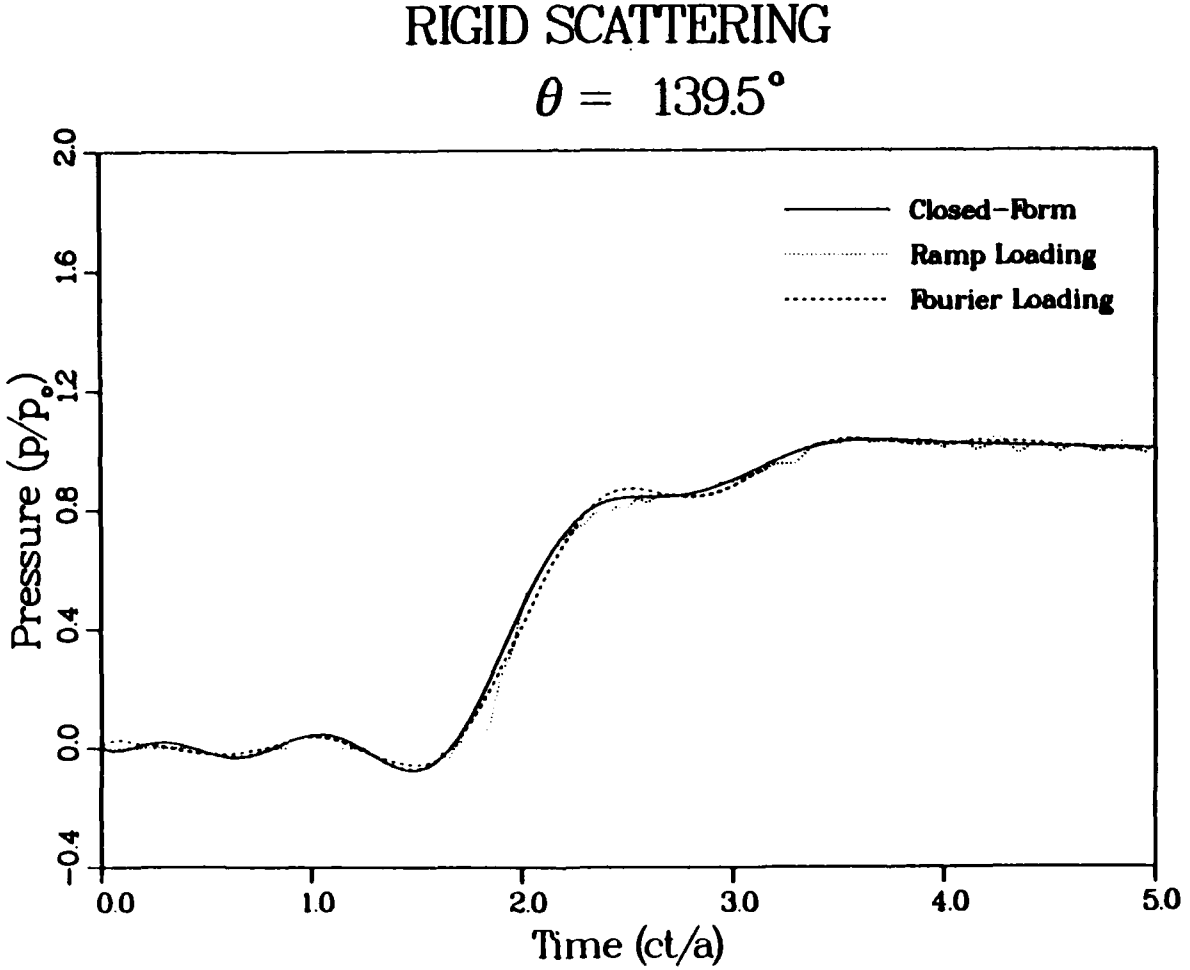
RIGID SCATTERING
θ = 139.5°
Closed-Form
Ramp Loading
Fourier Loading
Pressure (p/p₀)
2.0
1.6
1.2
0.8
0.4
0.0
-0.4
0.0
1.0
2.0
3.0
4.0
5.0
Time (ct/a)

Fig. 6c

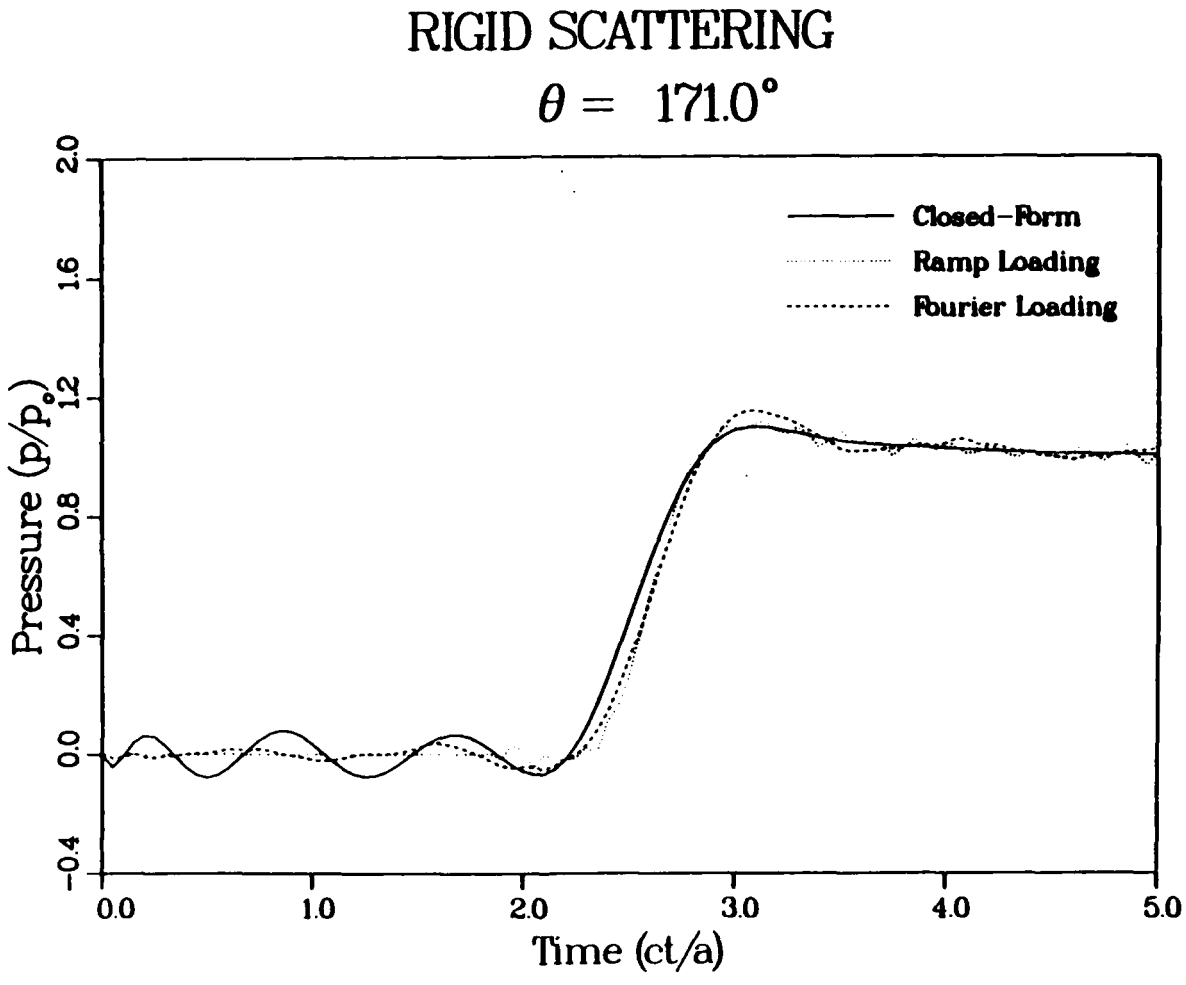
RIGID SCATTERING
θ = 171.0°
Closed-Form
Ramp Loading
Fourier Loading
Pressure (p/p_o)
2.0
1.6
1.2
0.8
0.4
0.0
-0.4
0.0
1.0
2.0
3.0
4.0
5.0
Time (ct/a)

Fig. 6f

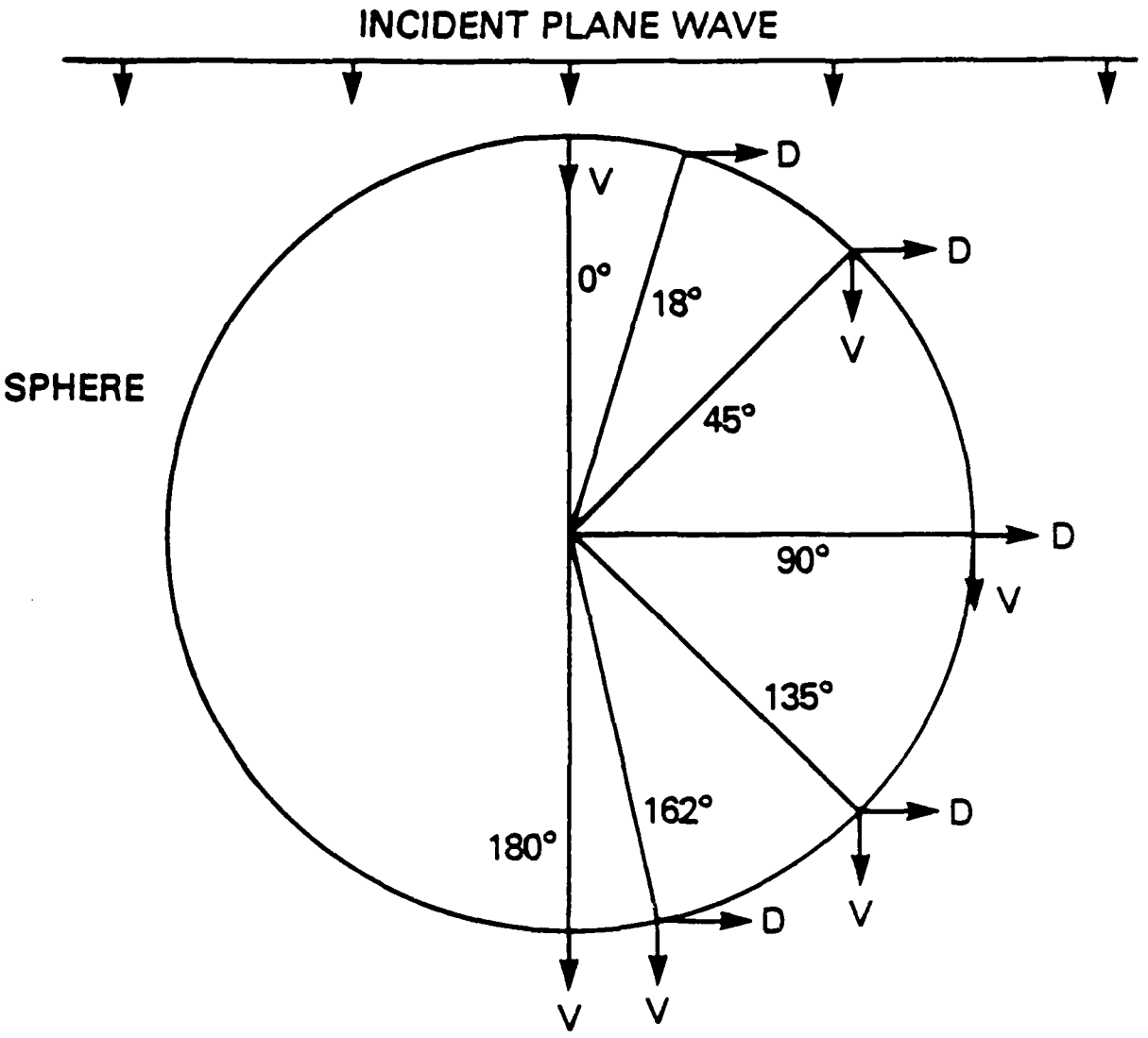

Fig. 7 — Locations and directions of plotted displacements and velocities

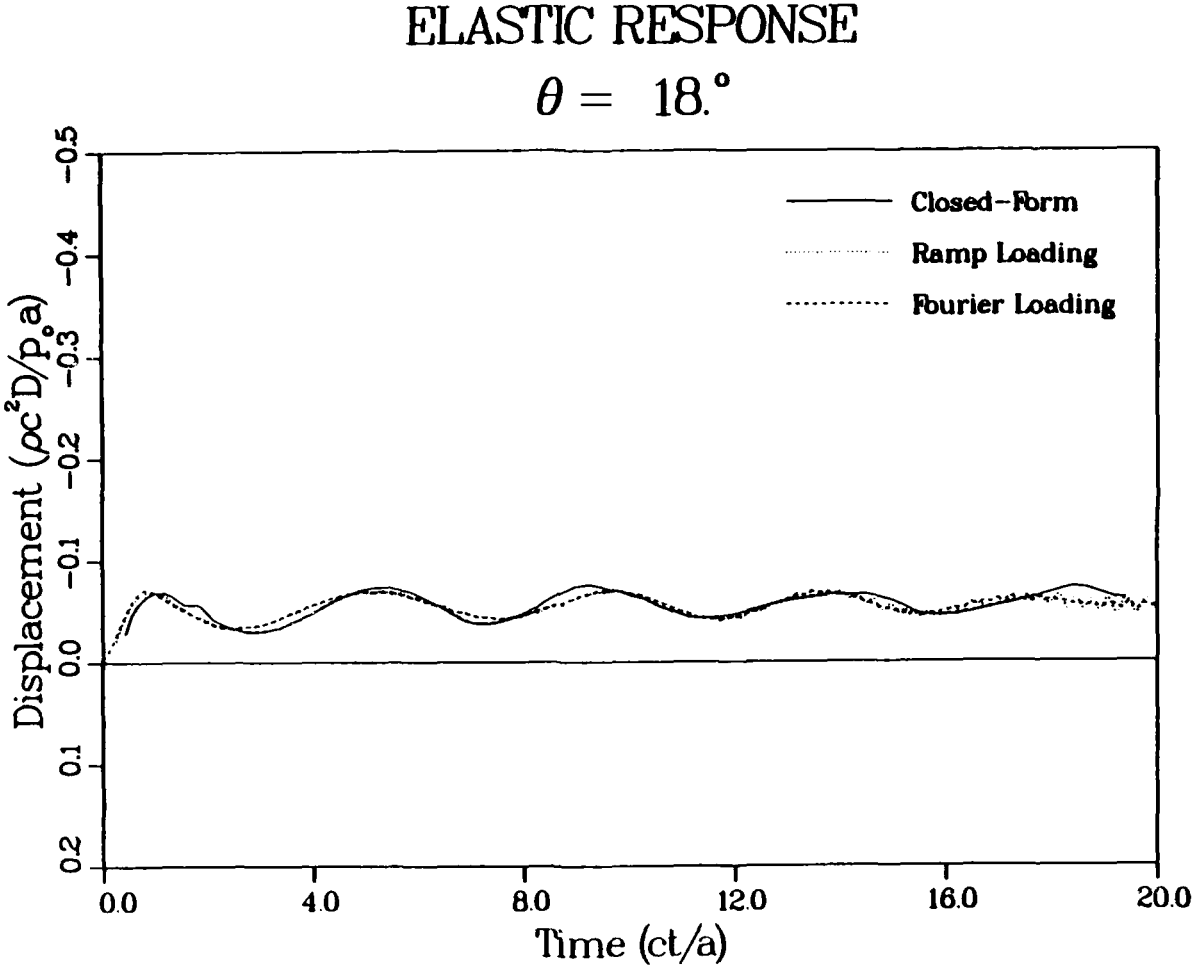
ELASTIC RESPONSE
θ = 18.°
Closed-Form
Ramp Loading
Fourier Loading
Displacement (ρc²D/p₀a)
-0.5
-0.4
-0.3
-0.2
-0.1
0.0
0.1
0.2
0.0
4.0
8.0
12.0
16.0
20.0
Time (ct/a)

Fig. 8a

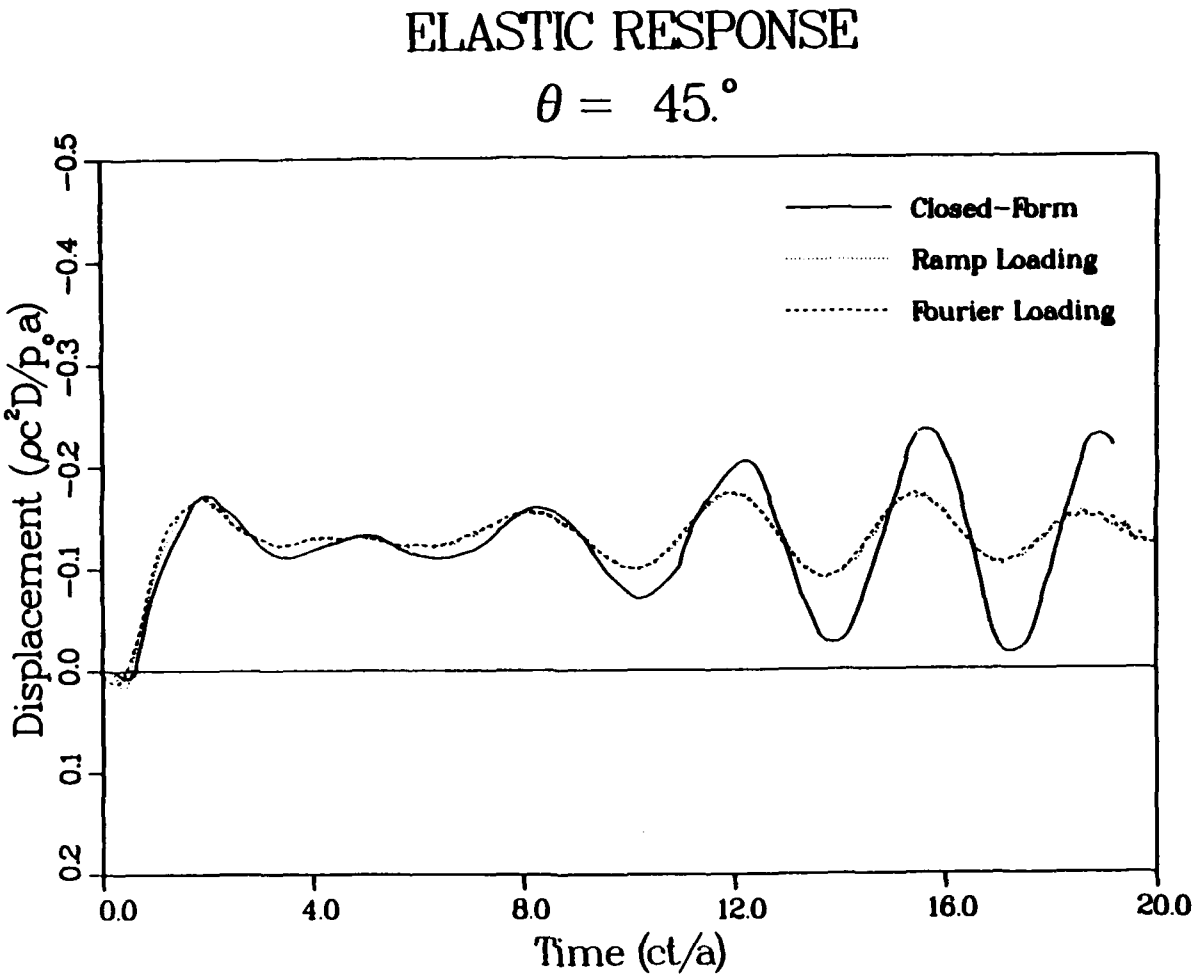
ELASTIC RESPONSE
θ = 45.°
Closed-Form
Ramp Loading
Fourier Loading
Displacement (ρc²D/p₀a)
-0.5
-0.4
-0.3
-0.2
-0.1
0.0
0.1
0.2
0.0
4.0
8.0
12.0
16.0
20.0
Time (ct/a)

Fig. 8b

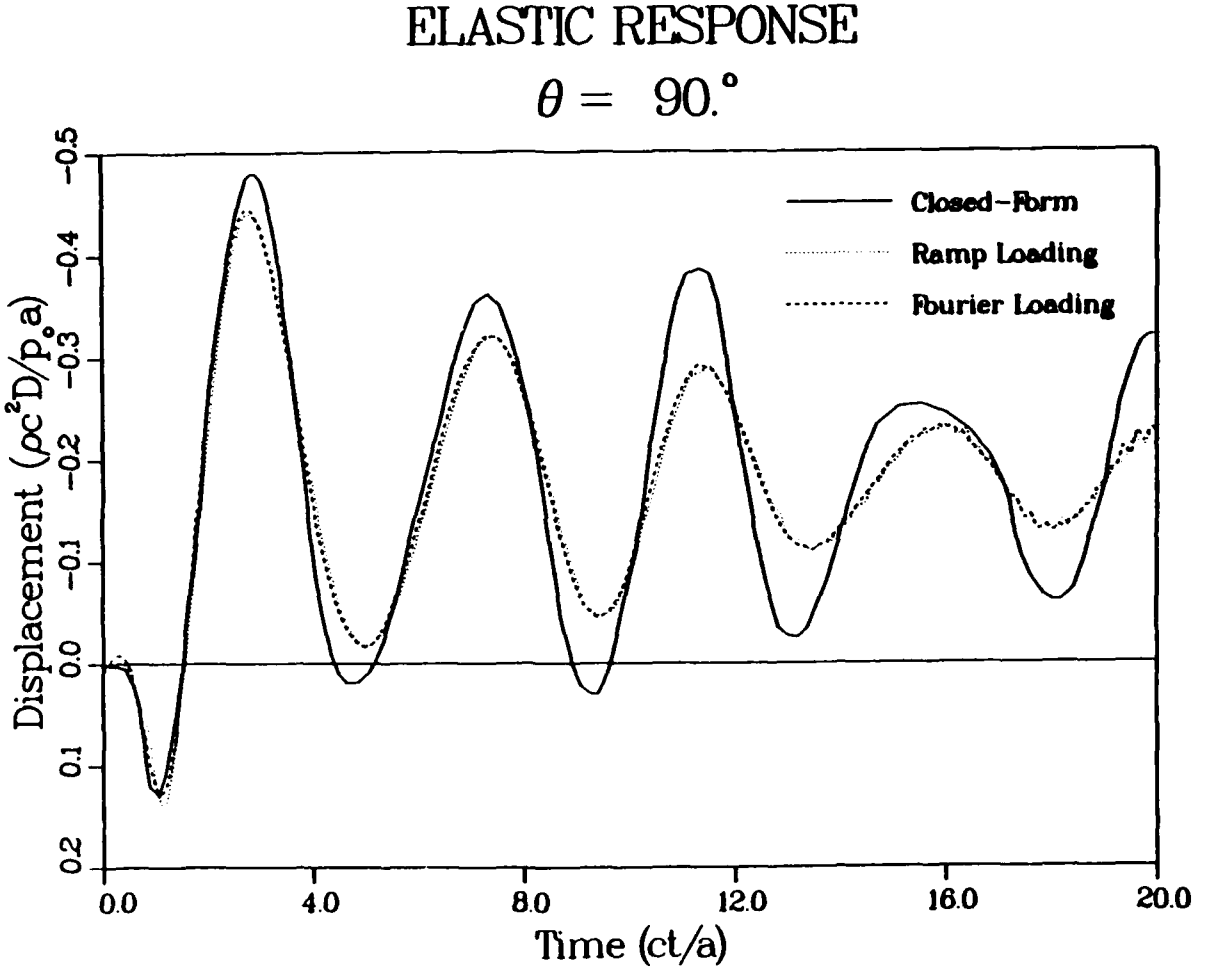
ELASTIC RESPONSE
θ = 90.°
Closed-Form
Ramp Loading
Fourier Loading
Displacement (ρc²D/P₀a)
-0.5
-0.4
-0.3
-0.2
-0.1
0.0
0.1
0.2
0.0
4.0
8.0
12.0
16.0
20.0
Time (ct/a)

Fig. 8c

ELASTIC RESPONSE

$\theta = 135.°$

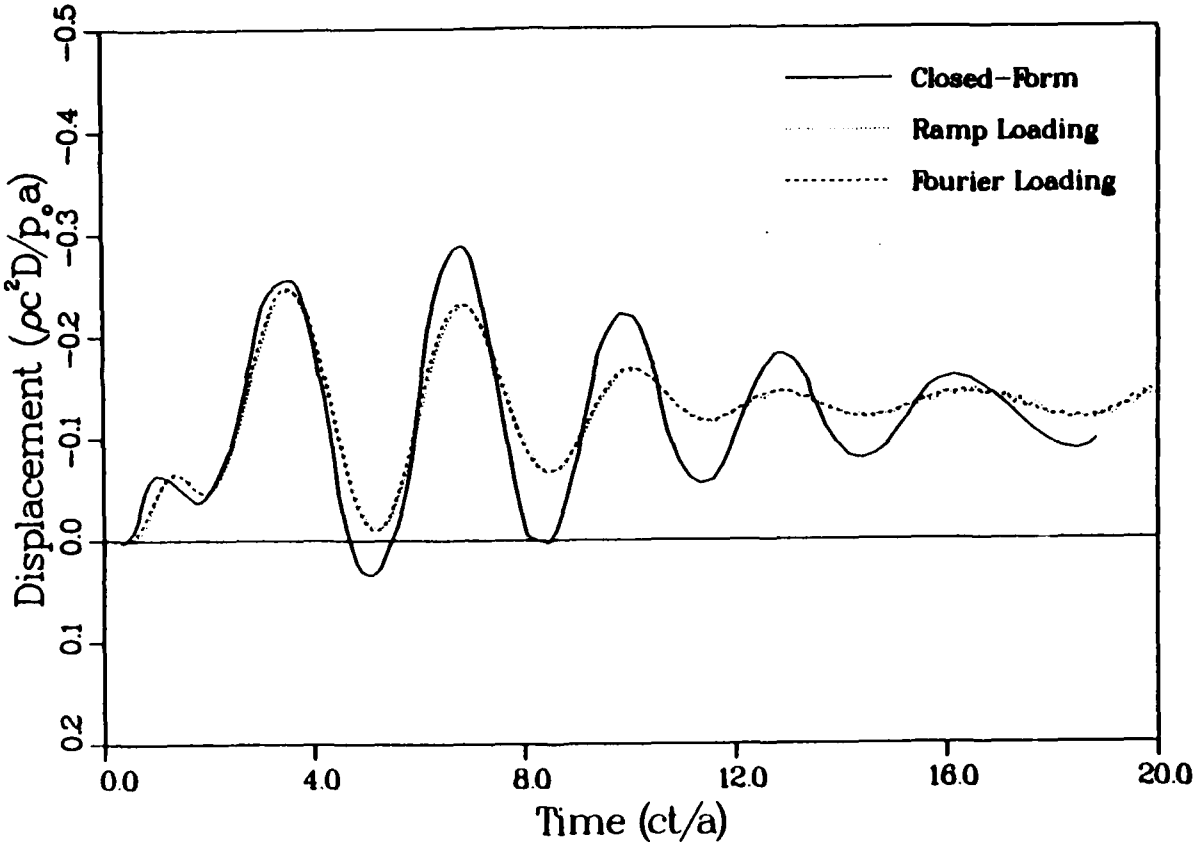

Fig. 8d

ELASTIC RESPONSE

$\theta = 162.°$

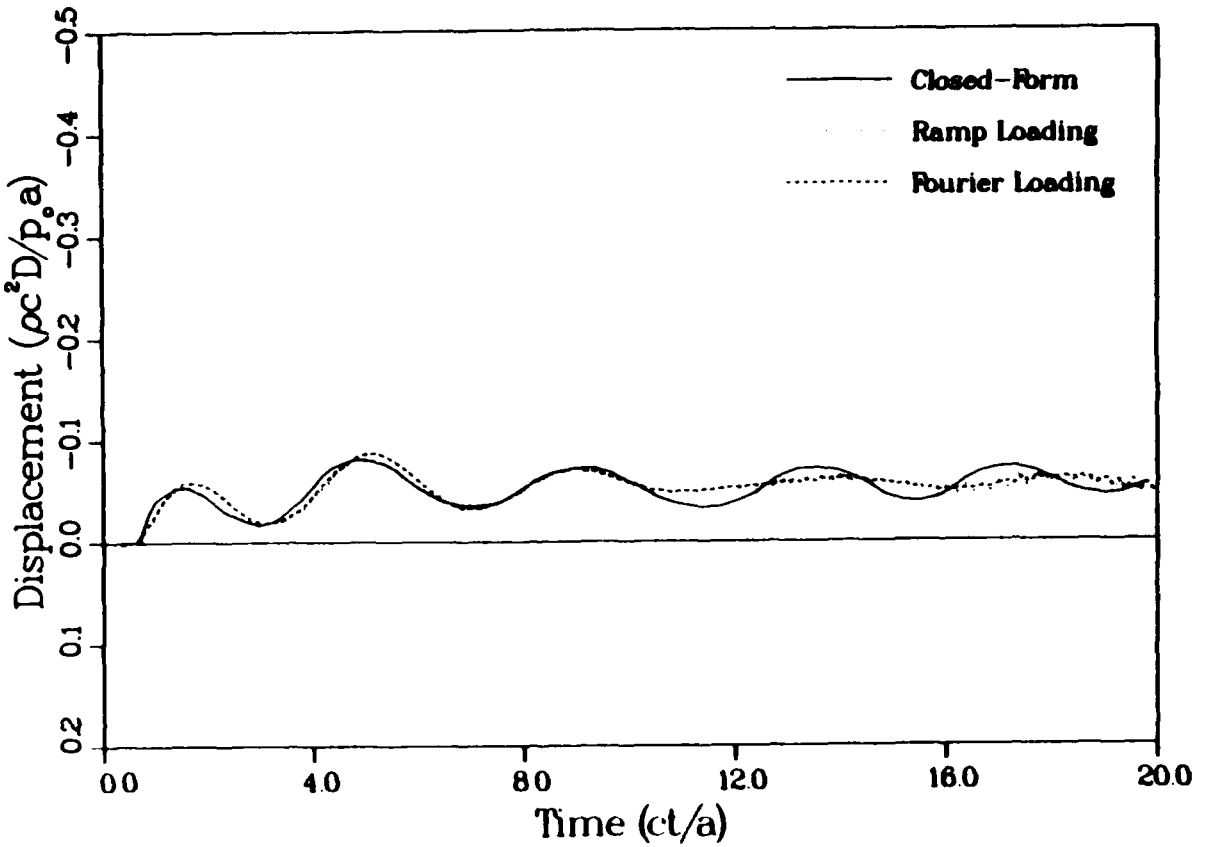

Fig 8c

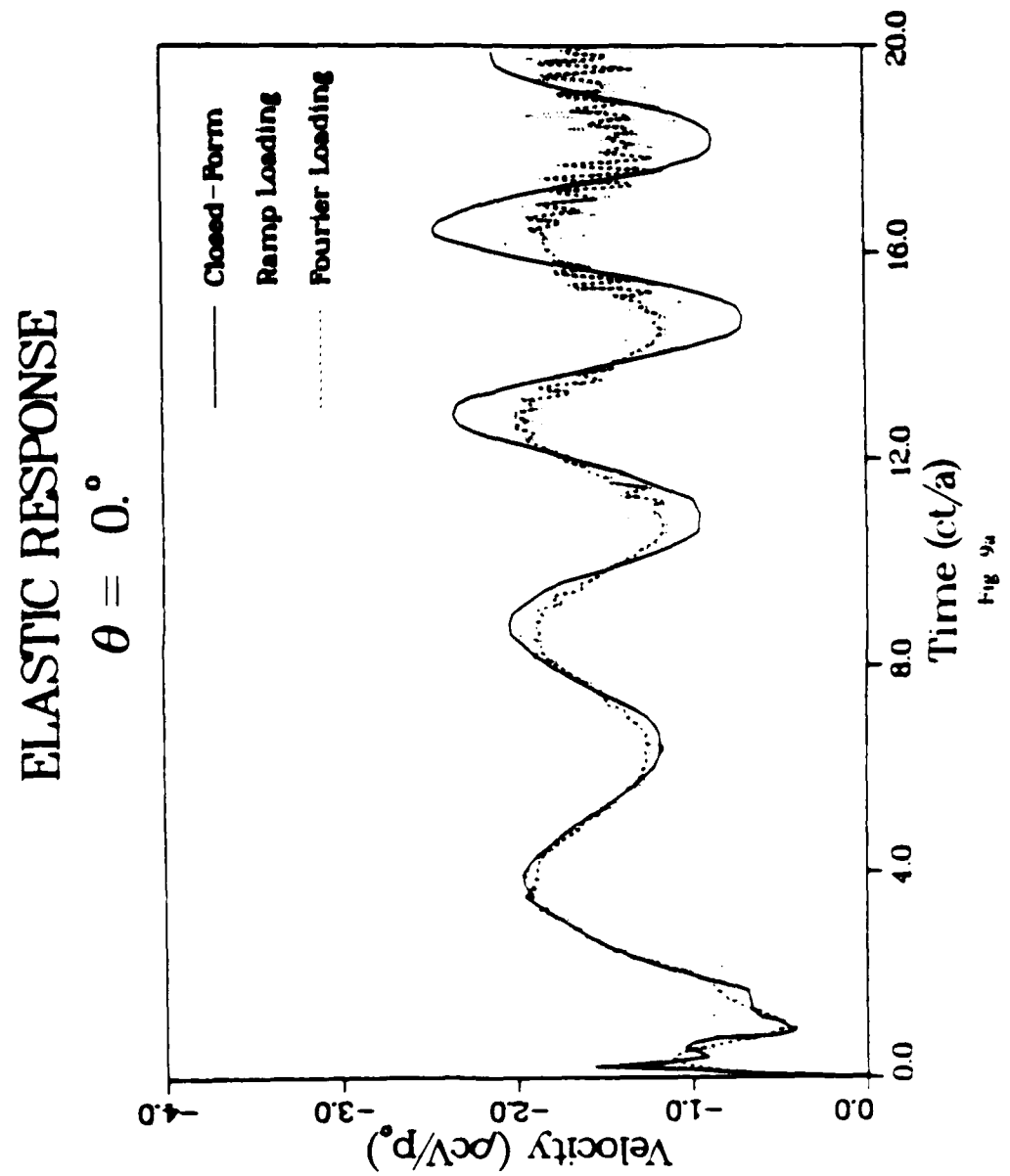
ELASTIC RESPONSE
$\theta = 0.°$
Closed-Form
Ramp Loading
Fourier Loading
Velocity ($\rho c V/p_o$)
0.0
-1.0
-2.0
-3.0
-4.0
0.0
4.0
8.0
12.0
16.0
20.0
Time (ct/a)

Fig 9a

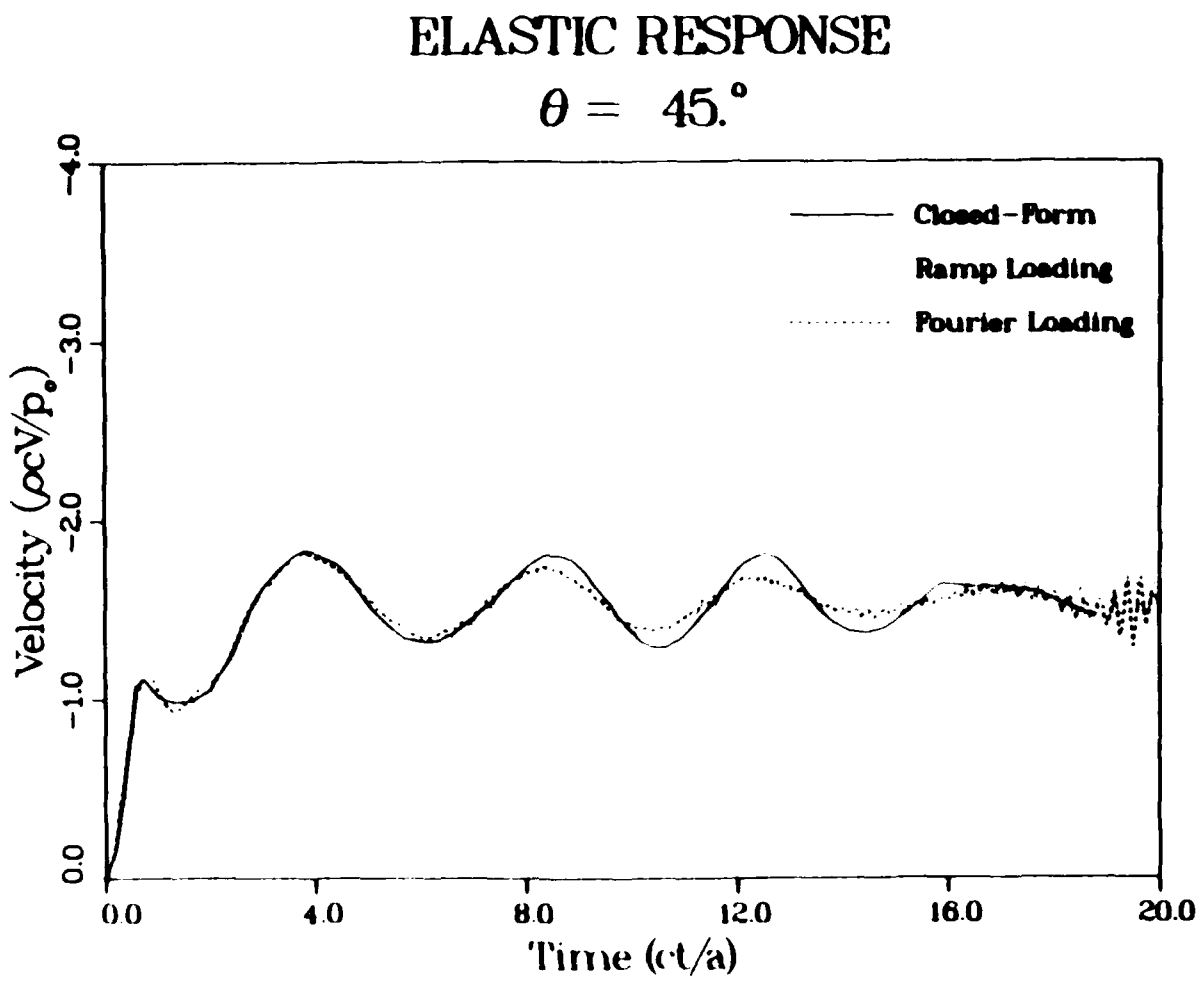
ELASTIC RESPONSE
θ = 45.°
Closed-Form
Ramp Loading
Fourier Loading
Velocity (ρcV/p₀)
0.0
-1.0
-2.0
-3.0
-4.0
0.0
4.0
8.0
12.0
16.0
20.0
Time (ct/a)

Fig. 9b

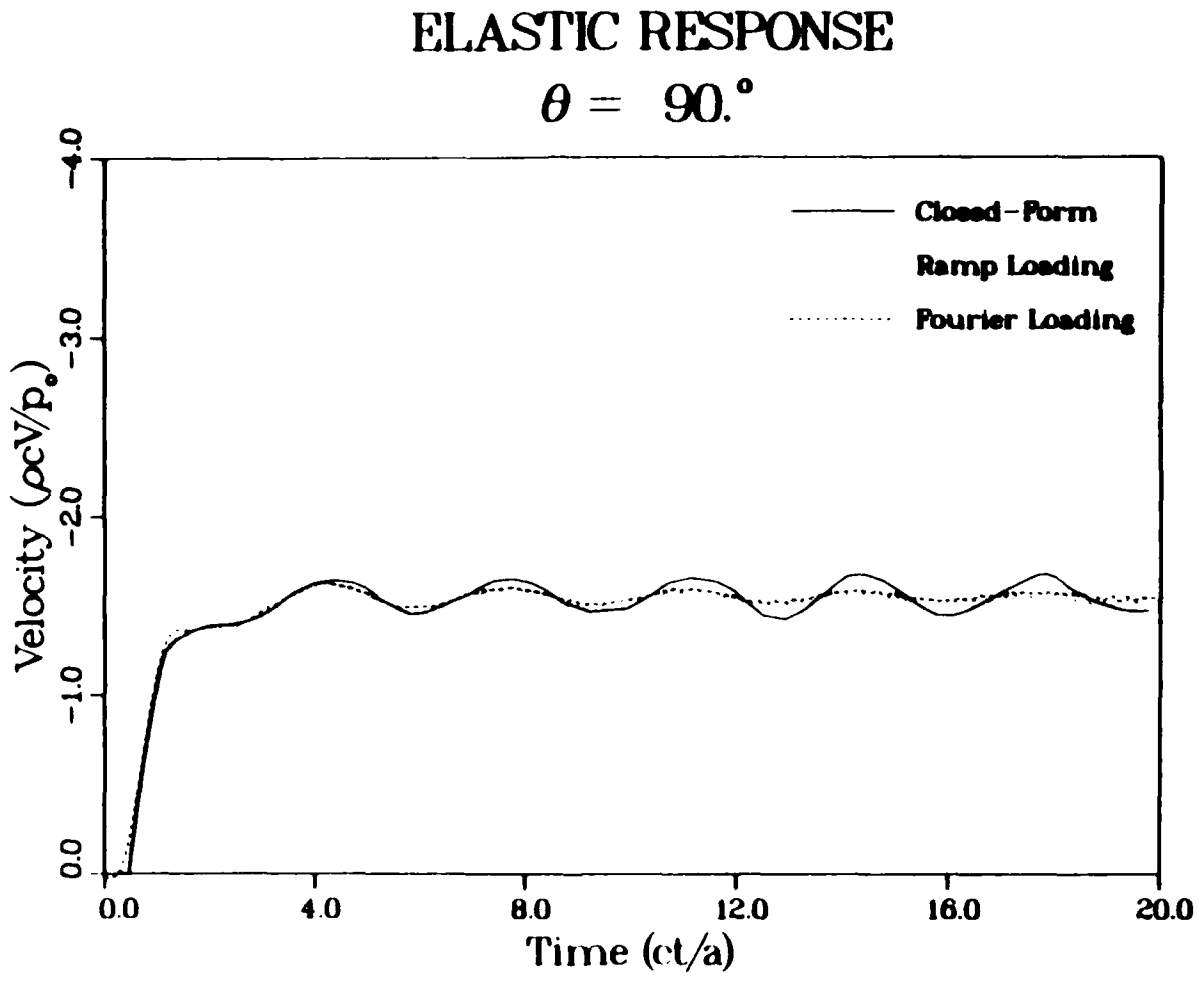
ELASTIC RESPONSE
θ = 90.°
Closed-Form
Ramp Loading
Fourier Loading
Velocity (ρcV/p₀)
0.0
-1.0
-2.0
-3.0
-4.0
0.0
4.0
8.0
12.0
16.0
20.0
Time (ct/a)

Fig 9c

ELASTIC RESPONSE

$\theta = 135.^{\circ}$

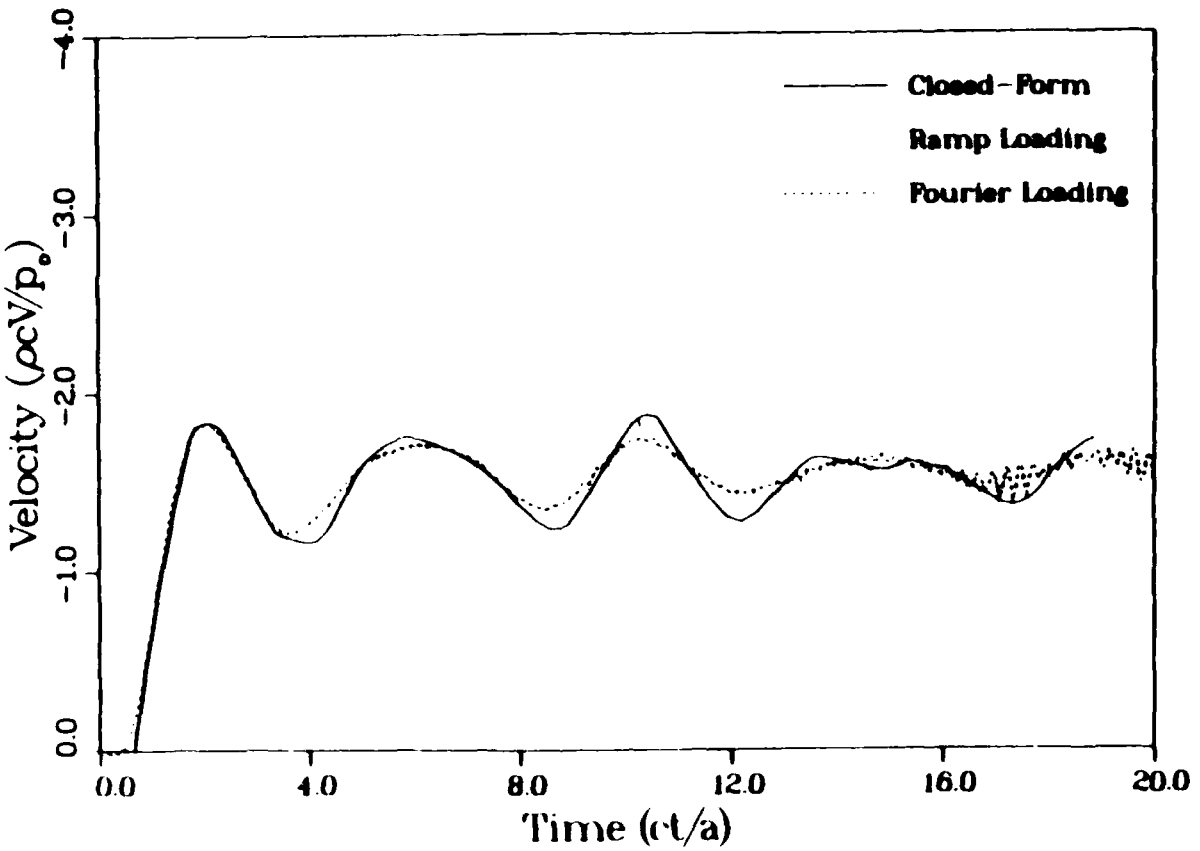

Fig 9d

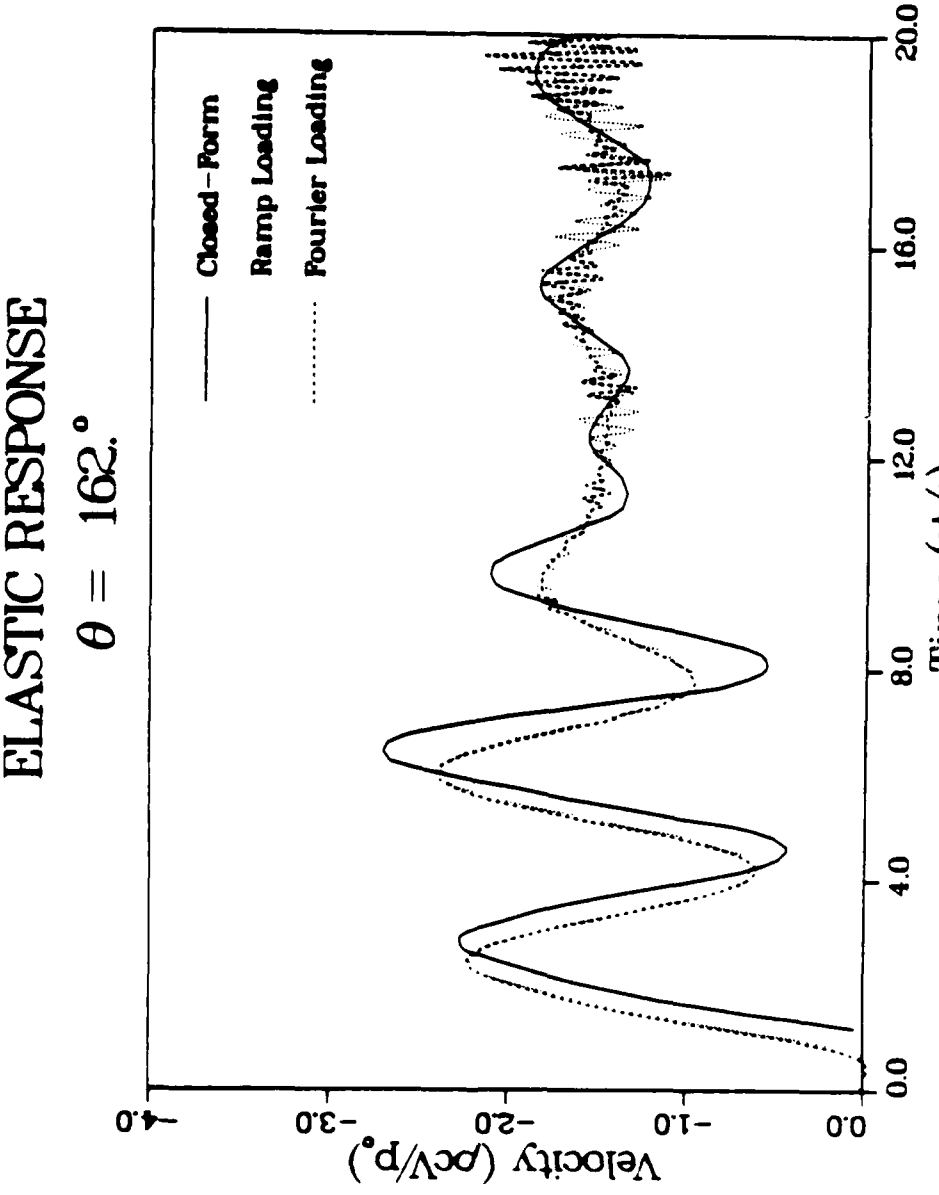
ELASTIC RESPONSE
θ = 162.°
Closed-Form
Ramp Loading
Fourier Loading
Velocity (ρcV/P₀)
Time (ct/a)
0.0
-1.0
-2.0
-3.0
-4.0
0.0
4.0
8.0
12.0
16.0
20.0

Fig. 9c

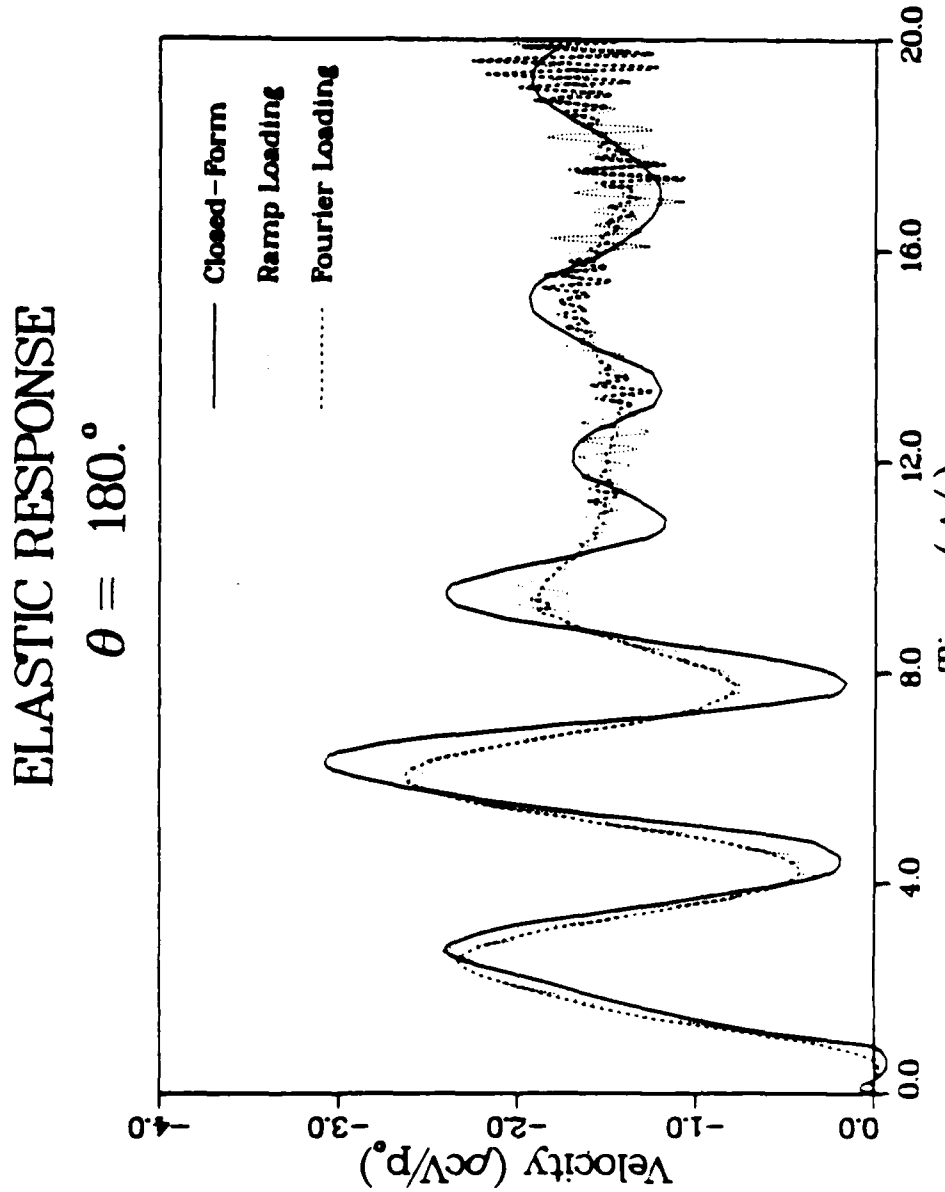
ELASTIC RESPONSE
$\theta = 180.^\circ$
Closed-Form
Ramp Loading
Fourier Loading
Velocity ($\rho cV/p_o$)
0.0
-1.0
-2.0
-3.0
-4.0
0.0
4.0
8.0
12.0
16.0
20.0
Time (ct/a)

Fig. 9f

END

8-87

DTIC